PROCESS PARAMETER INFLUENCE ON HIGH CYCLE FATIGUE LIFE OF DIRECT METAL LASER SINTERED PARTS

A thesis proposal presented to the faculty of the Graduate School of
Western Carolina University in partial fulfillment of the
requirements for the degree of Master of Science in Technology

By

Riley W. Seyffert

Advisor: Dr. Sudhir Kaul
School of Engineering + Technology

Committee Members:
Dr. Patrick Gardner, Rapid Center, College of Engineering and Technology
Dr. Wes Stone, School of Engineering + Technology

May 2019

ACKNOWLEDGEMENTS

First and foremost, I would like to thank my parents for their boundless support in my relentless endeavors. Without them, I wouldn't be close to the person I am today. You guys have raised me to perfection and the least I can do is give you endless gratitude as I tackle life's challenges.

I would like to thank the entire team at the Rapid Center. Dr. Patrick Gardner- The majority of my skills have been taught while under your wing. The lessons you have taught me will stay with me for my entire life and I am eternally grateful. Monty Graham- Thank you for putting up with all of my nonsense questions and pestering. Without your support, I would not be able to accomplish any of this. Brett Banther- I strive to become at least half the engineer you are today. Whether you know it or not, all those little tricks you've taught me will stick with me throughout my career and I couldn't thank you enough. Shawn Lyvers- Without your electrical support, I would have half the thesis that I have today. Thank you for dealing with my seemingly everlasting novice questions and always helping me out. Mike Clare- Observing your ability as a design engineer will stick with me for years to come.

Last, but not least, I would like to thank my thesis committee for their support throughout my graduate education. Dr. Sudhir Kaul- Without your wealth of knowledge and continuous support, I would not be able to accomplish any of this, thank you. Dr. Wes Stone- The skills you have taught me, whether be in class or for thesis support, will help carry my career as a successful engineer, thank you. Dr. Patrick Gardner- You've helped me so much, you've managed to make it onto this list twice, thank you.

TABLE OF CONTENTS

LIST OF TABLES

LIST OF FIGURES

ABSTRACT

PROCESS PARAMETER INFLUENCE ON HIGH CYCLE FATIGUE LIFE OF DIRECT METAL LASER SINTERED PARTS

Riley W. Seyffert, M.S.T.

Western Carolina University (March 2019)

Advisor: Dr. Sudhir Kaul

Direct metal laser sintering (DMLS) is a relatively new additive manufacturing (AM) technique. This manufacturing process involves fusing powdered metal layer by layer by using a high-powered laser. Although AM is expected to significantly transform the manufacturing process, there are some limitations that restrict the speed at which parts can be manufactured through the DMLS process. This study focuses on comprehending the influence of process parameters, and parameter interactions, involved in additive manufacturing by using an EOS M290 DMLS machine. A design of experiments is conducted to investigate process parameter in order to determine adequate parameters, or interactions, that can assist in comprehending the DMLS manufacturing process. The parameters tested in this study are layer thickness, laser scan speed, and laser hatch distance. These parameters have been primarily chosen because of their influence on build time. The response variables of the design of experiments include results from dynamic testing through cyclic fatigue. Fatigue testing data is obtained from a custom fatigue testing machine built specifically for this study. Additionally, tensile testing has been conducted to determine ultimate tensile strength.

It can be concluded from the results of this study that layer thickness is a significant parameter that needs to be carefully evaluated for fatigue life consideration. The other two parameters tested in this study, scan speed and hatch distance, are seen to be statistically insignificant. Out of all possible parameter interactions tested in this study, the only statistically significant interaction between parameters is that of layer thickness and scan speed. Results from tensile tests conclude that ultimate tensile strength does not seem to be significantly affected by any process parameter. These results highlight the fact that while the static material properties may not be affected by different process parameters, the same conclusion cannot be made about the influence of process parameters on high cycle fatigue characteristics.

CHAPTER ONE: INTRODUCTION

This chapter provides an overview of this research along with contextual information about additive manufacturing. A problem statement and a brief outline of this study have been included in this chapter. This chapter also provides the motivation behind this research and its potential importance to the industry efforts in implementing the direct metal laser sintering (DMLS) process as a manufacturing process.

1.1 Additive Manufacturing - Introduction

Conventional manufacturing processes have been extensively used for many years, many of these processes are subtractive in nature. Processes such as forging, casting, and machining have undergone many changes but the fundamentals of these processes have not changed. These processes resulted from the industrial revolution, and these days many industry analysts believe that we are entering a manufacturing revolution due to the widespread use of additive manufacturing. As technology advances, so does the level of manufacturing complexity. Gas turbine blades are a fine example of current manufacturing limitations. The design of a gas turbine blade is becoming more advanced than the processes used to manufacture a gas turbine blade. Conventional manufacturing of these advanced designs can be time-consuming and expensive. Recently, additive manufacturing (AM) has been gaining popularity in the manufacturing environment because of the potential capabilities AM possesses when it comes to advanced manufacturing. There are many different types of AM that are being currently used but the main idea behind AM consists of building layer by layer. The computer-aided design (CAD) model is sliced into layers with processing software and sent to an AM machine that produces the part, one layer at a time. Usually, the process involves extruding a thin string of the desired

material in the shape of the part until a layer is formed. The build plate then drops down by the thickness of the layer, and then another layer is extruded upon the subsequent layer until the building process is complete.

Direct metal laser sintering (DMLS) is a relatively new AM technique. This manufacturing process involves fusing powdered metal layer by layer by using a high-powered laser. This process works by laying down a thin layer of metal powder and sintering that powder to the previous layer and then repeating the process. Once the layer sinters to the previous layer, a recoating blade brings a new layer of metal powder across the build plate, and the process repeats until the building process is complete. DMLS provides a reduction in material waste and can mitigate tooling wear during production [1]. This benefit, along with part fabrication occurring in a controlled, automated environment means that DMLS requires less production time and labor than conventional manufacturing methods [1]. This process allows for manufacturing much more intricate designs and the intricate designs can consist of internal geometries that may not be possible through a conventional machining or forging processes.

Since DMLS is a relatively new process, there has not been a significant number of studies to qualify DMLS as a means of a full-time manufacturing production option. This is particularly because the process has been generally limited to the development of prototypes. There are studies in the literature that indicate that the bending fatigue performance comparison between DMLS and cold-rolled parts shows good visual agreement between 2×10^5 and 2×10^6 cycles to failure [2]. In the same study [2], two different vendors were used when obtaining the DMLS parts for testing. Each vendor's test parts used different process parameters to build the parts, yielding different results. The need to choose appropriate process parameters (scanning strategy of the laser beam, powder deposition, etc.) to enhance the density of the part and avoid

imperfections has been discussed in the literature [3]. Currently, the DMLS manufacturing process is very time consuming, and AM technologies have generally been applied in product development rather than production since the build speed is too low [4]. Arguably, this could change in the future with a better understanding of the influence of process parameters and with an increase in the build speed.

Although AM is expected to significantly transform the manufacturing process, there are some limitations that restrict the speed at which parts can be manufactured through the DMLS process. The main focus of this study is on comprehending the influence of process parameters that are involved in additive manufacturing by using an EOS M290 DMLS machine located in the Center for Applied Technology on campus of Western Carolina University. This study investigates some of the critical process parameter by using a design of experiments to find the adequate combination of parameters that could allow DMLS to become a viable means of manufacturing. The output variable of this design of experiments includes results from dynamic testing to test for high cycle fatigue life. Since an existing fatigue testing setup is not readily available, a significant part of this study involves the design and fabrication of a fatigue testing machine that performs three-point bending for a cyclic fatigue test.

1.2 Scope of Thesis

A review of the literature pertaining to additive manufacturing, specifically direct metal laser sintering, has concluded that there is a limited number of studies to validate the effects of the process parameters in the building process. Some studies have investigated fatigue properties of DMLS parts but these studies have concluded that a better understanding of the influence of process parameters would lead to a better understanding of the fatigue life of parts made by

DMLS [2]. This study seeks to shed some light on the role that different process parameters play in material properties as well as to answer the following research questions:

1. Can DMLS be used to manufacture parts that are equivalent to other processes while expediting the manufacturing speed?
2. What process parameters (such as layer thickness, scan speed, laser hatch distance, etc.) can be used to minimize the build time while maintaining the static structural properties of a part?
3. What process parameters can be used to minimize the build time while maintaining the dynamic structural properties of a part?

The main goal of this study is to find the process parameters that can be used to produce parts at a much quicker pace while still maintaining adequate static and dynamic properties that are equivalent to parts made through conventional manufacturing. The results of this study are expected to assist in understanding the use of DMLS in manufacturing complex parts in a production environment.

1.3 Overview of Thesis

This thesis seeks to answer the research questions stated above by performing a series of tests at different parameter sets. This series of tests is in the form of a design of experiments. The process parameters investigated in this study are laser scanning speed, layer thickness, and laser hatch distance. Each parameter has a high and a low value to form a two level, three factor full factorial design of experiments with three replicates. The values chosen for laser scan speed are 1083 mm/s for the low value and 1245 mm/s for the high value. The high value for laser scan

speed is 15% above the default scan speed of 1083 mm/s. The low value for layer thickness is also the default of the DMLS machine at 0.02 mm. The high value for layer thickness is 100% higher than the default, at a value of 0.04 mm thickness. The low value for hatch distance in this study is chosen to be the default setting, 0.09 mm. The high setting for laser hatch distance is 0.1 mm. These values have been determined to stay within a specific energy density with the use of an energy density calculation adopted from EOS. The energy density model that has been used to obtain these values can be found in the mathematical model discussed in Chapter 3 of this document. Validation of the results from the design of experiments consists of high cycle fatigue testing conducted on a fatigue testing machine built specifically for this study. This thesis contains all the information regarding the design and fabrication of this fatigue testing machine. Once the machine was built, testing has been conducted and conclusions have been drawn to enhance the understanding of process parameters and their role in fatigue life of parts made through direct metal laser sintering. Additionally, tensile testing has been conducted to determine process parameter influence, if any, on static material properties such as ultimate tensile strength.

The next chapter, Chapter 2, of this thesis provides a literature review for contextual information about additive manufacturing and DMLS. This chapter also discusses other studies that are relevant to the research done for this study. Chapter 3 discusses the mathematical model used for this study, providing necessary calculations that have been performed to select process parameters and to build the fatigue testing machine. Chapter 4 discusses all the results from testing and analysis. Chapter 5 draws overall conclusions and provides some directions for future research.

CHAPTER TWO: LITERATURE REVIEW

This chapter provides an overview of the literature related to this study to provide contextual information in support of the multiple aspects of research related to the content of this thesis. The first section provides a review of the history of additive manufacturing, this includes some brief examples of the capabilities of additive manufacturing such as stereo-lithography, fused deposition modeling, and direct metal laser sintering. Since this study primarily investigates direct metal laser sintering (DMLS), most of the literature discussed in this chapter is related to the DMLS process. This includes studies in the past that have reviewed process parameters and their influence on parts produced by DMLS. A brief discussion on design of experiments and fatigue testing is also presented.

2.1 History of Additive Manufacturing

The conventional manufacturing methods such as casting, forging, or machining have been very important means of manufacturing parts for mass production over the last century. These manufacturing methods have been able to adapt to increasing automation and modern manufacturing. The last three decades have seen rapid advances in computer-aided design and computer-aided manufacturing with a simultaneous reduction in the product development timelines. Due to these rapid advances, manufacturers have been investigating digital manufacturing technologies, starting with rapid prototyping and extending to mass production. One relatively new way of manufacturing complex geometries that has received increasing attention is additive manufacturing (AM), commonly referred to as 3-D printing. The first commercial use of AM can be traced back to the 1980's with the use of stereo-lithography (SLA) by 3D Systems [5]. This process involves controlling a laser to solidify ultraviolet (UV) light-

sensitive resin one layer at a time [5]. A significant impact on additive manufacturing was the commercialization of fused deposition modeling (FDM) in 1991 by Stratasys [5]. FDM involves building a part layer by layer just like SLA but by a fundamentally different process. Each layer is built by extruding a thermoplastic material in filament form to produce the final part [5]. Processes like SLA and FDM were the first AM processes that made an impact in the initial days of this manufacturing process. Around 1995, the FDM and SLA processes began to gain traction and these processes evolved rapidly. In 1996, Stratasys introduced a new type of FDM process that extruded a wax filament as opposed to a thermoplastic filament [5]. This advancement of printing technology continued and the printers coming out became more affordable to consumers, however the process was limited to manufacturing polymer parts only. In 1999, the first printer that could manufacture metal parts began to surface. In April 1999, Extrude Hone AM introduced its first metal printer that was used to print metallic parts at Motorola [5]. This process was based on inkjet technology and was adopted from printers based on research conducted at MIT. This inkjet technology is similar to a conventional inkjet printer used for printing text. At around the same time, the first powder-based selective laser-melting system (SLM) was introduced by Fockele & Schwarze, Germany. The turn of the century brought many new AM processes. In April 2000, Objet Geometries of Israel debuted an upgraded version of the UV curable inkjet printer that used 1,536 nozzles to dispense the UV curable resin [5]. During the same time frame, Z Corp introduced the world's first commercially available multi-color 3D printer called the Z402C. In July 2000, Stratasys began producing parts with ABS plastic by utilizing the FDM process. By 2002, Stratasys sold this type of printer to consumers for $29,900 [5]. Rapid advances have been made ever since, for a further detailed history of additive manufacturing, refer to [5].

2.1.1 Direct Metal Laser Sintering

Direct metal laser sintering (DMLS) is a recent addition to the growing list of additive manufacturing processes. The same company that manufactures the DMLS machine that this study is based on, Electro Optical Systems (EOS), introduced its first commercial DMLS machine at EuroMold 2003 [5]. DMLS can be described as "a powder bed fusion process used to make metal parts directly from metal powders…" (ASTM F2792). This fusion process consists of a high-powered laser that is controlled by a computer to sinter each layer of powdered metal, one layer at a time. Usually, the process consists of three different chambers. The first chamber is the dispensing platform, where the raw powdered metal material is held. The next chamber is where the build plate is found. This is where the laser sinters each layer of powdered metal. The final chamber is the collector bin. This is where the excess powder is collected during the re-coating process. The process can be summed up by the following: Step one consists of extending the dispensing platform by an increment of the selected layer thickness. Then, a re-coating blade travels across the dispensing chamber, gathering all the powder material for the current layer, and re-coats that layer onto the build plate. The excess powder is collected in the collector platform. The next step is for the laser to sinter the layer of powdered metal based on the geometry of the sliced part at that layer. This process is repeated until the full geometry is built.

A major factor to consider when it comes to implementing a process such as DMLS into a manufacturing line is part density. Due to the nature of the build process, parts produced by DMLS are nearly 100% dense, but not quite. Studies have shown that the majority of porosity develops in the outer layer of the printed material, but porosity on the inside is also present [6]. Many times, parts produced by DMLS are post-processed by heat treatment to increase the density of the part. This is done because DMLS parts usually contain microstructures with non-

equilibrium phases as well as very high residual stresses [6]. These non-equilibrium phases can consist of un-sintered powder or partially sintered powder. Studies have also shown that the process parameters involved with the build process must be carefully selected to produce adequate part density [4].

Building parts by DMLS instead of conventional manufacturing methods can result in a reduction in material waste and possibly mitigate issues such as tooling wear during production [1]. DMLS is also capable of producing parts that can be much more complex without requiring expensive tooling. Some examples of parts with increased complex internal geometries that can be produced by DMLS include heat exchangers and small-scale, internally cooled turbine rotors located inside a gas turbine engine [1]. In addition to creating twisted and contorted shapes, parts can be made with variable wall thicknesses, blind holes, internal thread features, and a very high strength-to-weight ratio. All these features have raised a high level of interest in this manufacturing process, however the rate of producing parts is currently considered to be an obstacle to produce parts for mass production. Since this manufacturing process is relatively new, it is necessary to understand the role played by multiple process parameters associated with this manufacturing process [7].

2.2 DMLS Process Parameters

Some of the most important aspects of a manufactured product are its mechanical properties, dimensional and shape accuracy, and surface roughness [7]. These aspects can be significantly influenced by the choice of process parameters. Some examples of these process parameters involved in DMLS include laser power, scanning speed of the laser, hatch angle, hatch distance, and build orientation. There is no ideal combination of process parameters that will build perfect parts. In fact, many of these process parameters influence each other [7]. For

example, increasing the layer height to reduce the build time could have a staircase effect on the finished product. This is when the layers of sintered powdered metal can be visible to the naked eye and on angled geometries, these layers resemble steps in a staircase. This staircase effect can have a direct negative effect on part dimensional accuracy and an increased surface roughness [7].

Build orientation is an important factor that can influence the amount of support material and subsequently affect the amount of wasted material. The support structure does not contribute towards the final part, wasting both build time and material [7]. It can also affect post-processing costs and mechanical properties [7]. Build orientation is highly dependent on the geometry of the part as well. For instance, when attempting to build a cylindrical part, the machine will print with much less support if the part is oriented straight up as opposed to laying down. The machine needs to support any overhanging features that pass a certain angle to build the part without failure. Improper build orientation causes anisotropy of the tensile properties of the built part, and therefore the placement and angle of rotation on the platform must be chosen to optimize the functionality of the part being produced [7].

During the sintering process, the laser beam moves line after line several times until the current layer of the part is fully sintered. This distance between each line is referred to as the hatch distance [8]. This parameter has a major influence on the laser's ability to fully sinter each layer of powder. The hatch distance is usually set to about a quarter of the diameter of the laser beam and if this is not maintained, the operator runs the risk of having un-sintered powder inside the part being built. Studies such as [8] conclude that hatch distance is a major contributing factor to surface finish, and it is also concluded [8] that a large hatch density can enhance mechanical strength due to more energy being absorbed into the part during the build process.

The density, along with many other material properties, can be altered by altering the process parameters. Laser scanning speed and laser power are two parameters that can have a direct effect on part density [4]. When increasing the laser scan speed, the power of the laser must be increased as well to ensure proper density of the part. For aluminum parts, increasing the laser scan speed without increasing the laser power can equate to a reduction of density by approximately 5% [4]. This is because porous voids are left within the part that contain un-sintered powder material. The power of the laser must be enough to fully sinter all the powder during each scan to ensure no powder is left un-sintered.

AM technologies such as DMLS are currently used in the prototyping environment mostly as compared to mass production due to the slow rate at which parts can be produced [4]. The literature indicates that the production of parts produced by DMLS can be possibly increased by tweaking some of the process parameters. In one study, [4], the build rate to produce AlSi10Mg parts was found to have increased by using a 1kW laser. Increasing the laser power allowed increasing the building speed of 5 mm^3/s to approximately 21 mm^3/s for AlSi10Mg [4], in this study a decrease of production time was not found to affect the mechanical properties in any way. Parts produced at 21 mm^3/s ended up with a hardness of approximately 145 HV 0.1 and a tensile strength of around 400 MPa which was found to be comparable to parts made through conventionally manufacturing processes [4]. This indicates that there may be some scope for process parameter optimization in DMLS.

2.3 Design of Experiments

The design of experiments (DOE) is a commonly used statistical methodology for analyzing process parameters. “A DOE is a method of experimenting with the complex interactions among parameters in a process or product with the objective of optimizing the

process or product" [9]. The process of conducting a DOE can be summed up in the following steps [10]:

- Identification of factors through experimentation by evaluating their significance to the responses and determination of their impact. The results of experiments are analyzed statistically.
- Statistical identification of factors with little to no influence.
- Determination of the values of significant factors and finding optimum settings, if possible.

A full factorial design of experiments is often used to determine all possible main effects as well as all possible parameter interactions [9]. When there are time limitations, a full factorial DOE is often replaced by a fractional factorial DOE. This allows a reduction in the total number of tests that need to be carried out but may result in some confounding. When conducting a fractional factorial design, it is important to carefully select the test configurations since it is possible that certain interaction effects could be missed [9].

Another careful consideration when designing a set of experiments is the selection of factors, or parameters, that should be tested. Process factors can be summed up into two categories; control factors and noise factors [11]. In operating or environmental conditions, the selection of factors that should be considered as control factors has a heavy influence on the conclusions that be drawn from the test data [11]. Often times, noise factors are not controllable. For example, a design of experiments to evaluate effects on gas mileage might have control variables such as travel speed, tire pressure, or octane levels but an example of a noise factor in this scenario might be the weather during the day of testing or the condition of the road being traveled on.

The series of experiments involves using different levels of the process parameters to determine the level that is most adequate for the application. For instance, laser power will be one of the process parameters investigated in this study by using two settings (or levels) of this parameter. Different test samples are made with each level of laser power and then validated by static and dynamic testing to determine which level of laser power has the least influence and which one has the most influence on the outcome or response.

Further validation for process parameter influence can be evaluated by fitting a regression model to the DOE data. A linear regression model is used to determine the association between two or more variables [12]. The results from the DOE can be evaluated by observing whether parameters or parameter interactions have a positive or negative effect on the outcome. Once a model is formed, the control parameters can be used to estimate the outcome, or response, of the test. This approach is only valid for parameters that fall within the domain of the selected study [13]. The strength of the regression model, or line of best fit, can be determined by the regression coefficient, or R^2, value [12]. The higher the R^2 value, the closer the data falls near the line of best fit.

2.4 Fatigue Testing

This section discusses the different aspects of fatigue testing that is necessary to determine the number of cycles to failure. Development of fatigue testing can be complex due to the influence of multiple variables on such a test.

2.4.1 Dynamic Testing

A three-point bending test for cyclic fatigue can be conducted per ASTM E466, "Standard Practice for Controlled Amplitude Axial Fatigue Tests of Metallic Materials" [14]. This standard covers the procedure for the performance of axial force controlled fatigue tests to

obtain the fatigue strength of metallic parts [14]. Such testing is typically carried out to obtain the number of cycles to failure at multiple loads, allowing the development of an S-N curve that can be used for design. The S-N curve plots the reversible stress amplitude against the number of cycles to failure. A typical S-N curve is plotted on a logarithmic plot and can be used to determine the fatigue limit of a material. For engineering materials, such as steel and titanium, the S-N curve becomes horizontal at a certain limiting stress, this is considered to be the fatigue limit, or endurance limit [15]. At this limit, usually 10^6 to 10^8 cycles to failure for ferrous metals, it is presumed that the part has infinite life [15].

This study focuses on high cycle fatigue, meaning that the number of cycles to failure is made up of the number of cycles to initiate a crack and the number of cycles to propagate the crack completely through the test sample [15]. This approach is adequate for determining if a part will fail or not but in order to gain a better understanding on crack growth throughout the failure cycle, a low cycle fatigue analysis should be conducted.

The S-N curve typically captures the high cycle fatigue characteristics at zero mean stress [15]. Adjustments are necessary if the loading does not occur with zero mean stress, this is particularly necessary in the presence of tensile mean stresses. When the mean stress is zero, the maximum and minimum stress amplitudes are equal [15]. A high cycle fatigue test can be carried out with the part being stationary and the load varying, or alternately one can achieve the same result with a stationary load and a moving test sample. For instance, the test specimen can be attached to an actuator to deliver the reciprocating force or the test specimen can be held in a fixture. The forces applied on the test specimen will cause tension on one side of the neutral axis and compression on the other side of the neutral axis. When the actuator retracts, the regions

under tension and compression get swapped, thereby resulting in reversible stress. This process can be repeated until the part fails.

2.4.2 Data Collection

The use of LabVIEW has been critical for this study to control the test set up while allowing an ability for data collection during the test. “LabVIEW is an innovative graphical programming system designed to facilitate computer-controlled data acquisition and analysis” [16]. The user interface panel of LabVIEW, referred to as the front panel, includes inputs that the user is able to change for the desired test such as frequency. The front panel can be customized to meet a user’s needs using graphical representations. These graphical representations can be viewed as the inputs of the system and alter the values that correlate to the changes in the outputs. Other than the front panel, or the user interface panel, there is a block panel that does all the work. For example, one could use a LabVIEW program that converts temperature from Fahrenheit to Celsius. In such a case, the front panel will have an input for the temperature in Fahrenheit and an indicator for the equivalent temperature in Celsius. On the block panel, the graphical representations of the formula used for the conversion can be seen. Using LabVIEW to control the fatigue testing set up has been important for this study.

2.5 Conclusions

This chapter provides necessary contextual information in support of the research carried out in this study. The discussion in this chapter includes background information about additive manufacturing, and the DMLS process in particular. Some background information about design of experiments and high cycle fatigue is also provided in this chapter.

CHAPTER THREE: MATHEMATICAL MODEL

This chapter presents the model that has been used before developing the experimental set up that is required for testing in this study. The results of the model were used to select the correct actuator for the fatigue testing machine while the fatigue calculations were used to predict the outcome of the experiment. The background model to calculate adequate energy density for each DMLS print is also presented in this chapter.

3.1 High Cycle Fatigue – Test Sample

A fatigue testing machine has been designed in this study to perform a three-point bending test on parts made of 316L stainless steel from the EOS M290 DMLS machine. The design of the test samples was based on the geometry found in the ASTM E466 standard [14]. A high cycle fatigue analysis was carried out to determine a range of loads that would be needed from the actuator in order to induce fatigue failure on the test samples. These calculations are presented in the subsequent sections of this chapter. Figure [3.1] shows the dimensions of the dog bone sample used in this study. A stress concentration was added in the form of a through hole in the middle of the test sample in order to reduce the number of cycles to failure to a reasonable limit. Since this study is particularly focused on comprehending high cycle fatigue, failure from 1000 cycles to 10^6 cycles is considered to be within the range of interest. However, the sample geometry was finalized in order to limit the number of cycles to failure to approximately 10,000. This was primarily done to accommodate a reasonable number of test samples for this study.

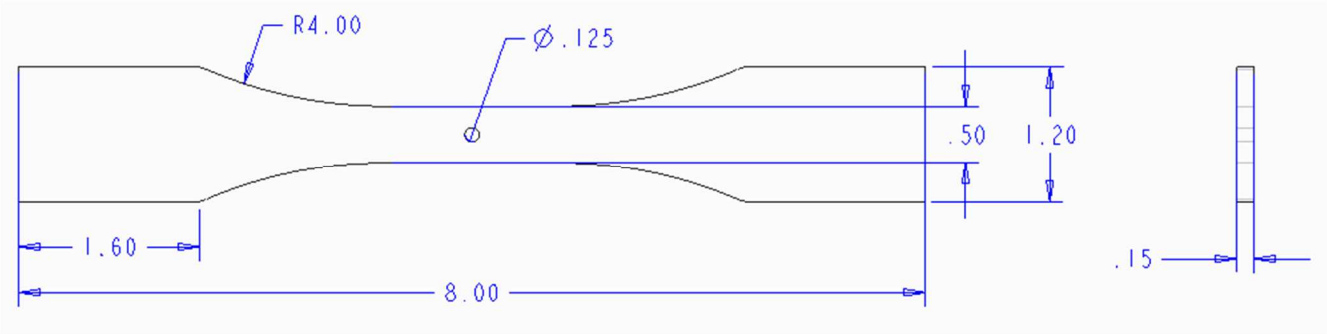

Figure [3.1]: ASTM E466 Test Sample Dimensions in Inches

3.1.1 High Cycle Fatigue -- Model

This section presents the governing equations used to estimate the number of cycles to failure for the test sample shown in Figure [3.1]. This model was used before building the fixture to have a reasonable estimate of the number of cycles to failure. The purpose of these calculations is to anticipate the results by plotting a modified SN (stress versus number of cycles to failure) curve and to identify the actuator settings that can be used to carry out the test.

The documented ultimate tensile strength of 316L stainless steel manufactured on an EOS machine is used to the endurance strength (S_e) and the strength corresponding to 1000 cycles (S_{1000}). The endurance strength correlates to 10^6 cycles to failure and the S_{1000} value correlates to 10^3 cycles for high strength steels. These values can be estimated as follows:

$$S_e = (0.5)(S_{ut}) \tag{3.1}$$

$$S_{1000} = (0.9)(S_{ut}) \tag{3.2}$$

The ultimate tensile strength, S_{ut}, used for Eq. (3.1) and (3.2) is obtained from the EOS data sheet for stainless steel 316L [17] and is 640 MPa. As a result, the calculated value for S_e was 320 MPa and the value for S_{1000} was calculated to be 576 MPa. These values can be used to plot an un-modified SN curve. Figure [3.2] shows the SN curve for the un-modified EOS 316L stainless steel.

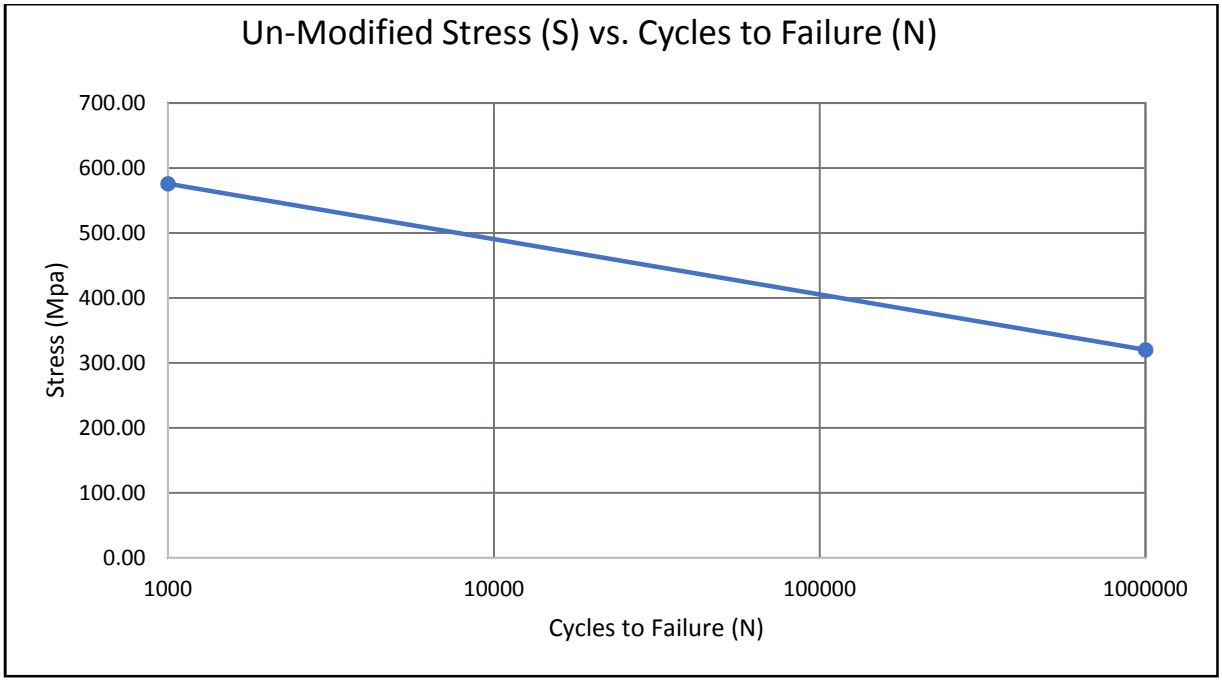

Figure [3.2]: Un-Modified S-N Curve for EOS 316L Stainless Steel

These values obtained from Eq. (3.1) and Eq. (3.2) are then used to calculate a modified endurance strength (S_{ed}) and modified S_{1000} value (S_{1000D}) by accommodating the adjusting factors as well as stress concentration effects. A modified endurance strength is necessary because it is assumed that the surface finish of the test sample will not be perfect along with

other deviations from the standard conditions. This involves using the endurance strength of 316L stainless steel and multiplying it by the size factor, load factor, and surface factor. The size factor compensates for the size of the test sample. Usually, the diameter value for the size factor is simply the diameter in mm but in this case since the test sample is a non-rotating rectangular section, a different diameter equation was used. This equation is a factor of the base and height of the test sample as opposed to the diameter. The load factor compensates for the type of load being exerted onto the test sample. These values can be 0.7 to 0.9 for an axial load, 0.577 for a torsion load, or in this case, the size factor equals 1, for a bending load. The surface factor compensates for the surface finish of the test sample. The surface factor equation for a machined finish has been used, this type of finish closely resembles the finish of a printed DMLS part without any post-processing. The calculation of the modified endurance strength is summarized in the following equations:

$$M_{size} = \left(\frac{d_e}{7.62}\right)^{-0.1133} \tag{3.3}$$

$$d_e = 0.808\sqrt{bh} \tag{3.4}$$

$$M_{load} = 1 \tag{3.5}$$

$$M_{surface} = 4.51 * {S_{ut}}^{-0.265} \tag{3.6}$$

$$S_{ed} = S_e * M_{size} * M_{load} * M_{surface} \tag{3.7}$$

The value obtained from the modified endurance strength in Eq. (3.7) was 260.4 MPa. The next step is to use the stress concentration factor (K_t) to define a fatigue notch factor (K_f). The notch sensitivity factor (q) is then calculated to define the relationship between K_t and K_f. Peterson equation in Eq. (3.8) was used to calculate the notch sensitivity factor, q. The value in

Eq. (3.9) is chosen because stainless steel 316L is determined to be a high strength steel (S_{ut} > 550 MPa). In Eq. (3.8), ρ is the diameter of the through hole in the test sample, this value is equal to 0.125 inches and can be found in Figure [3.1]. The corresponding equations are as follows:

$$q = \frac{1}{1 + \frac{\alpha}{\rho}} \tag{3.8}$$

$$\alpha = 0.025\left(\frac{2070}{S_{ut}}\right)^{1.8} \tag{3.9}$$

The next step, as discussed previously, is to use the notch sensitivity factor (q) to obtain the fatigue notch factor (K_f) with the help of a stress concentration factor (K_t). The stress concentration factor can be found from a semi-empirical chart in the literature [18] and is found to be 1.9 for the geometry shown in Figure [3.1]. This value corresponds to the stress concentration caused by the through hole incorporated into the test sample for a bending load and can be calculated as:

$$K_f = 1 + q(K_t - 1) \tag{3.10}$$

Once the fatigue notch factor is calculated, the modified endurance strength for the notched test sample can be calculated as follows:

$$S_{eD} = \frac{S_e * M_{size} * M_{load} * M_{surface}}{K_f} \tag{3.11}$$

The modified endurance strength for the notched member was calculated to be 194.5 MPa from Eq. (3.11). To calculate the modified S_{1000} value, the next step is to calculate the corresponding fatigue notch factor and the notch sensitivity factor (q_{1000}) that correlate to the S_{1000} value. Once these values are obtained, the modified S_{1000D} value for a notched member can be calculated per the following equations:

$$K'_f = 1 + q_{1000}(K_f - 1) \tag{3.12}$$

$$q_{1000} = 0.48\, ln\left(\frac{S_{ut}}{6.89}\right) - 2 \tag{3.13}$$

$$S_{1000D} = \frac{S_{1000}}{K'_f} \tag{3.14}$$

The S_{1000D} value for the notched test sample calculates to be 543.7 MPa. While the S_{eD} value corresponds to the stress level for the part to fail at 10^6 cycles, the S_{1000D} value corresponds to the stress for the part to fail at 10^3 cycles. The two values, S_{1000D} and S_{eD}, can be used to calculate the constants A and B for the governing model of the test sample. The modified SN curve can be plotted using the two constants by using the following equations:

$$S_{1000D} = A * (10^3)^B \tag{3.15}$$

$$S_{eD} = A * (10^6)^B \tag{3.16}$$

By solving for A and B in Eq. (3.15) and Eq. (3.16), the values are found to be B = -0.149 and A = 1520.1 MPa. These values can be plugged back into Eq. (3.15) and Eq. (3.16) in order to predict stress levels or the number of cycles to failure for the test sample used for this study.

They also govern the S-N curve (stress vs. cycles to failure) for DMLS 316L stainless steel. Figure [3.3] shows the S-N curves – un-modified as well as modified for the test sample being used in this study. The governing equations for the modified SN curve can be expressed as follows:

$$S = 1520.1 * N^{-0.149} \tag{3.17}$$

$$N = \left(\frac{S}{1520.1}\right)^{\frac{1}{-0.149}} \tag{3.18}$$

While Eq. (3.17) computes the reversible stress required for failure for a given number of cycles, Eq. (3.18) computes the number of cycles to failure for a given level of reversible stress. It may be noted that the model is valid only for reversible stress and only within a range of 10^3 cycles to 10^6 cycles.

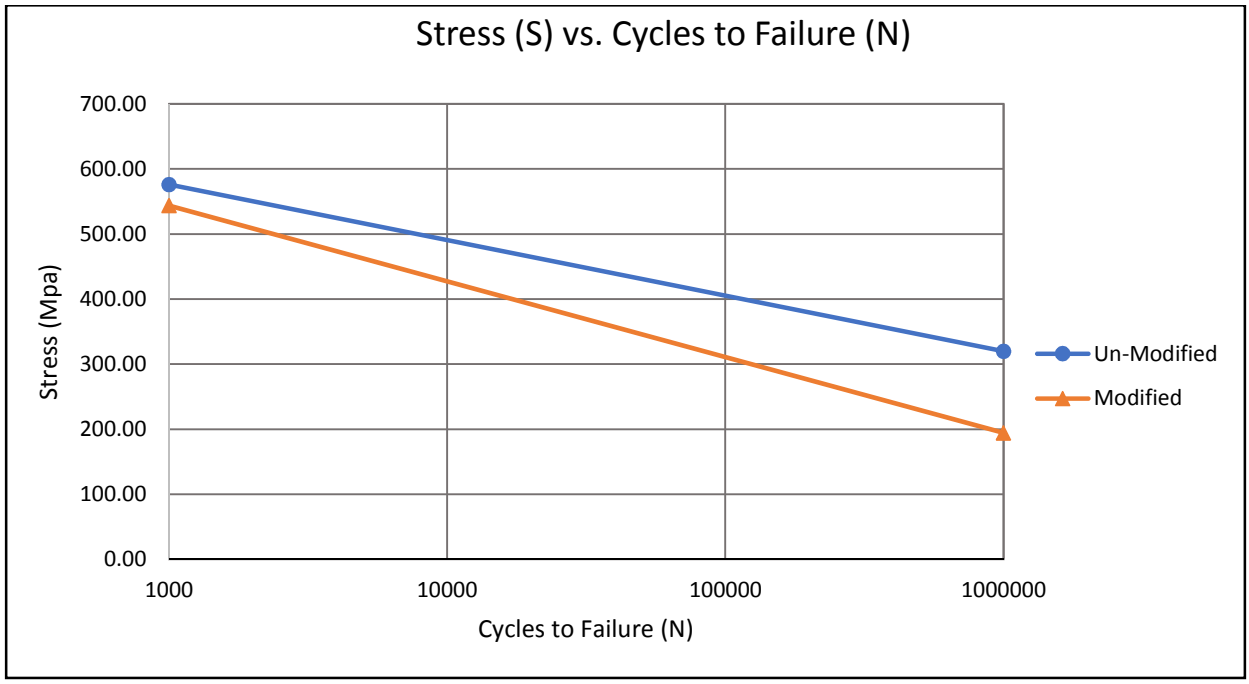

Figure [3.3]: Un-modified and modified SN curves for the test sample

The modified SN curve presented in this section allows the use of a reference model that can be used to estimate the loads needed to induce fatigue failure. These loads have also been used to choose the actuator needed for the test setup. The chosen actuator permits a wide range of forces that would allow 7,000 to 15,000 cycles to failure due to reversible fatigue loading. Table [3.1] shows the estimated number of cycles to failure, as predicted from the modified SN curve.

Table [3.1]: Stresses and Cycles to Failure

Number of Cycles to Failure (N)	Stress (Mpa)
1000	543.73
10000	385.97
100000	273.98
1000000	194.49

The final step in the fatigue model is to use the estimated stress to calculate the force required to induce failure. This has been done by calculating the bending moment diagram of the test sample and computing the force at the location of the stress concentration. A simply supported beam was used because of the simplicity of the design needed for the test set up. Eq. (3.19) provides the relationship between the stress (*S*) and the calculated force (*F*) as follows:

$$S = \frac{F\frac{l}{4} * \frac{h}{2}}{\frac{bh^3}{12}} \tag{3.19}$$

Eq. (3.17) was used to calculate the required stress to induce failure at 10,000 cycles by using the modified SN curve, this was calculated to be 386 MPa. Eq. (3.19) was used to calculate the corresponding force. A force of 58.3 lbf was calculated to induce 386 MPa of stress at the center of the test sample. As a result, the actuator was chosen to provide a reversible load approximately in the range of 59 lbf.

3.1.2 Fatigue Testing

For this study, all fatigue testing was conducted by using the fatigue testing machine that was fabricated in-house. Once the correct actuator was chosen, the rest of the fatigue testing machine was built around this actuator. The number of cycles to failure is the only value being measured in this test by using test samples built with varying parameters.

The fatigue test was automated by creating a VI in LabVIEW. The block diagram of the VI can be seen in Figure [3.4]. In the block diagram, there are two different systems for the actuator movement. The first system is to move the actuator into position. This system allows the user to move the actuator in small increments until it reaches the desired position, while starting the test. The distance of this movement is based upon the length of time that the signal is sent to the solenoid. For example, if the system is set to extend for half a second, the actuator will extend until the half a second time is over. If the user wants to move the actuator at a smaller increment, the user must shorten the time that the signal is sent to the solenoid. Once in position, the next system is implemented. This system is a loop that will continuously extend and retract the actuator until the test sample fails. Once the test is started, the system is set up to keep a cycle count every time the actuator extends, meaning that for every extension and retraction of the actuator, the cycle count increases by one. The frequency of the test system is controlled by the time the signal is being transmitted to the solenoid in the loop. The smaller the time, the quicker the system will extend and retract the actuator. All tests in this study were conducted at a frequency of 2.5 Hz.

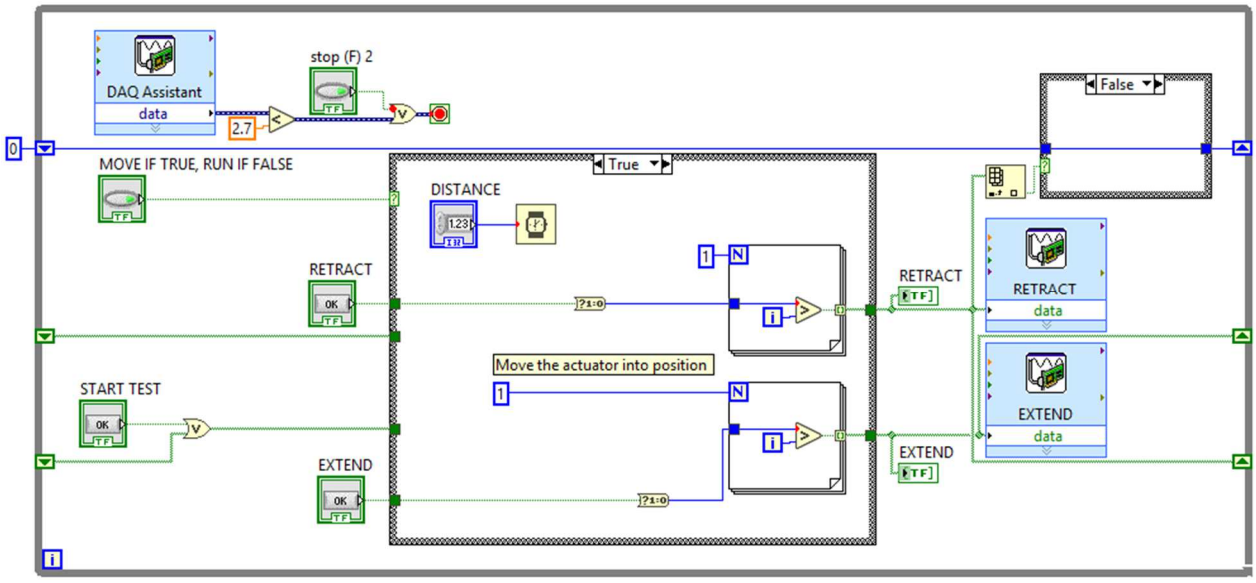

Figure [3.4]: LabVIEW Block Diagram

LabVIEW was used to output a signal to a data acquisition (DAQ) device in the form of a National Instruments USB-6008. This DAQ was used to transmit a signal from the virtual instrument to the directional control solenoid that in turn controlled the action of the actuator. Before the signal reached the control solenoid, it first went through a solid-state relay. The relay is important in this operation because the relay takes the external voltage from the DAQ and determines which solenoid to extend. This ensures that the solenoid will have separate signals for extending and retracting the actuator separately. The control valve is then connected to a tie rod cylinder and the actuator delivers the desired force onto the test sample.

The machine also incorporates a safety stop so the user can run tests without being present. This safety stop is in the form of a force sensor under the actuator. When the test sample breaks, the actuator is fully extended and applies force onto the force sensor. This force then changes the resistance of the force sensor, in turn changing the voltage reading from the force

sensor. This voltage difference is then read by the LabVIEW software and input into a stop command for the entire system. This stops the test when the test sample fails and this also stops the cycle counting as soon as the sample fails. A complete bill of materials of the test set up that was built in-house can be found in Table [3.2].

Table [3.2]: Fatigue Testing Machine Bill of Materials

Item	Vender	Part #	QTY
T-Slotted Framing Quad Rail, Silver, 3" High x 3" Wide, Solid (24")	Mcmaster.com	47065T806	24
T-Slotted Framing Corner Brace for 3" High Double and Quad Rail, 4-3/16" Long	Mcmaster.com	5537T194	1
T-Slotted Framing Extended Corner Bracket for 3" High Double and Quad Rail	Mcmaster.com	47065T254	2
Tie Rod Air Cylinder Cushioned, Double Acting, 1-1/4" Bore Size, 2" Stroke Length	Mcmaster.com	6491K222	1
Solenoid Air Directional Control Valve High-Flow, Spring-Return, Closed Center, 1/8 NPTF, 24V DC	Mcmaster.com	6425K173	1
Push-to-Connect Tube Fitting for Air Straight Adapter, for 1/8" Tube OD x 1/8 NPT Male (4)	Mcmaster.com	5779K102	4
T-Slotted Framing Steel End-Feed Fastener, for 1-1/2" High Single Rail (4 pack)	Mcmaster.com	47065T97	5
Flexible Standard Nylon Tubing Semi-Clear, 0.093" ID, 1/8" OD (per foot)	Mcmaster.com	5112K61	25
Muffler 1/8 NPT Male, Steel, 11 scfm @ 100 PSI Maximum Flow Rate	Mcmaster.com	4450K1	2
Industrial-Shape Hose Coupling Size 1/4, Zinc-Plated Steel Plug, 1/8 NPTF Male End	Mcmaster.com	6534K19	1
Solid state relay, panel mount, hockey puck style, 3-32 VDC input voltage, SPST, N.O. MOSFET, 12A contact rating, 3-200 VDC load voltage, DC Switching, LED indicator(s).	automationdirect.com	AD-SSR6M12-DC-200D	2
RHINO switching power supply, 24 VDC (adjustable) output, 1.46A, 35W, 120/240 VAC or 100-375 VDC nominal input, 1-phase, aluminum housing, panel mount, screw terminals.	automationdirect.com	PSS24-035	1
USB-6008 Low-Cost Multifunction I/O and NI-DAQmx	Ni.com	779051-01	1

For this study, fatigue testing is conducted at reversible stress, meaning that the mean stress is zero all through the test. This is made possible by pushing down on the test sample to produce a tensile stress on the bottom of the test sample and a compressive stress at the top, and then pulling up the test sample reverses the forces giving a compressive stress on the bottom of the test sample and a tensile stress on the top. An image of this simply supported set up can be seen in Figure [3.5]. Figure [3.6] shows a section view of the simply supported structure to give more details about the support structure used in the fatigue testing machine. These components were made from 6061 aluminum and the two edge fixtures were designed so that they can be connected to the fatigue testing machine on the rails of the 80/20 frame. Also, contained in Figure [3.5] and [3.6] is the test sample, shown as red.

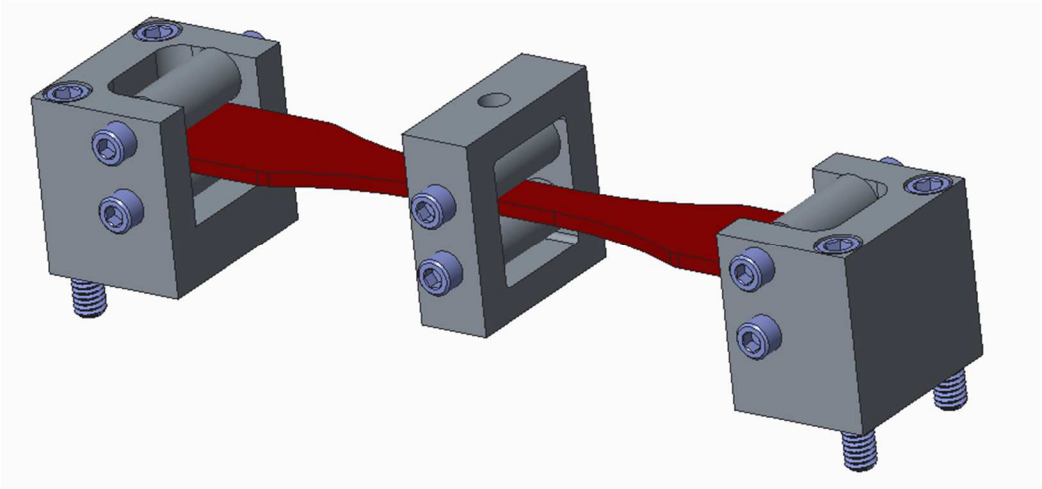

Figure [3.5]: Simply Supported Test Sample Frame

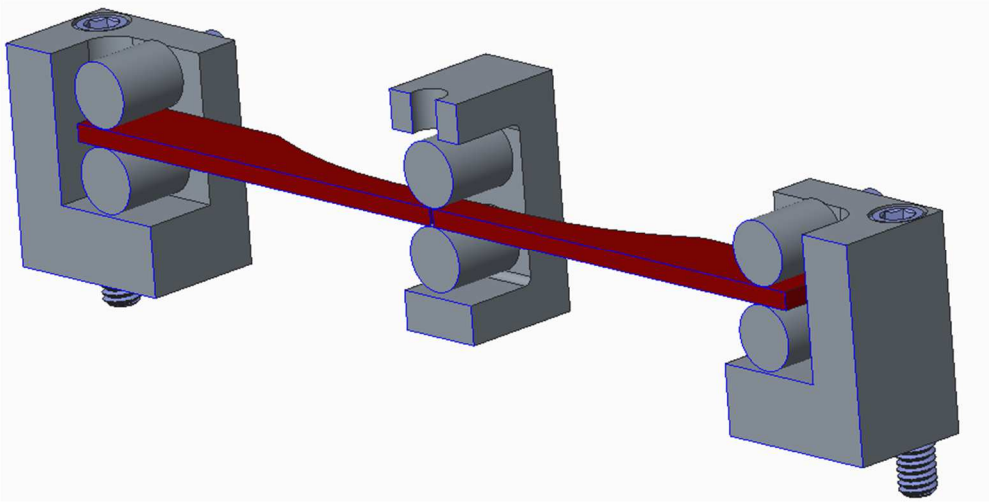

Figure [3.6]: Simply Supported Test Sample Section View

As stated above, the frame of the machine was constructed with two 12” pieces of 80/20 extruded aluminum. These pieces were held together with 80/20 brackets. The actuator is held into position with a 90 degree 80/20 bracket as well. A computer-aided design rendering of this fatigue testing machine can be found in Figure [3.7] with the actuator bracket is shown in black.

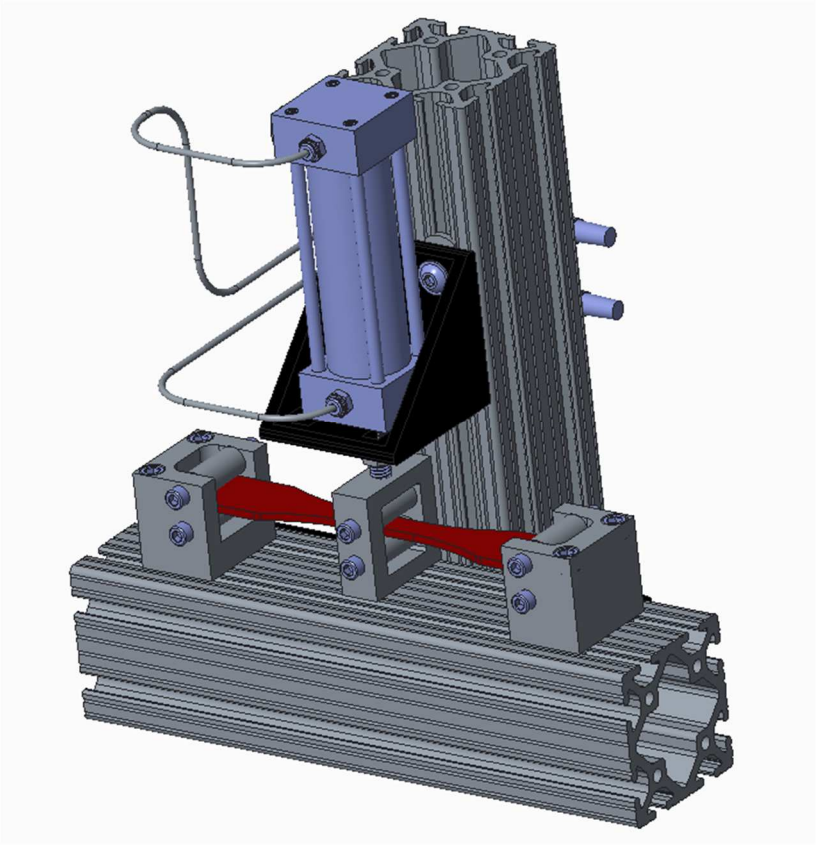

Figure [3.7]: Fatigue Testing Machine

3.2 Tensile Testing

Static tensile testing has been conducted in this study by using the Instron 5967 Universal Testing Machine. A picture of this testing machine can be found in Figure [3.8]. This test involves extending the test sample in tension until failure while recording the load needed to extend the sample. This test measures the load and the input deflection. Data acquired from this test can be plotted onto a stress vs. strain diagram. The stress vs. strain diagram can be used to obtain material characteristics such as the ultimate tensile strength, yield strength, or the modulus of elasticity. This test was carried out to compare the material characteristics of parts manufactured from DMLS 316L stainless steel with parts made from 316L stainless steel that

were manufactured via conventional manufacturing. This comparison can be used to determine static mechanical properties.

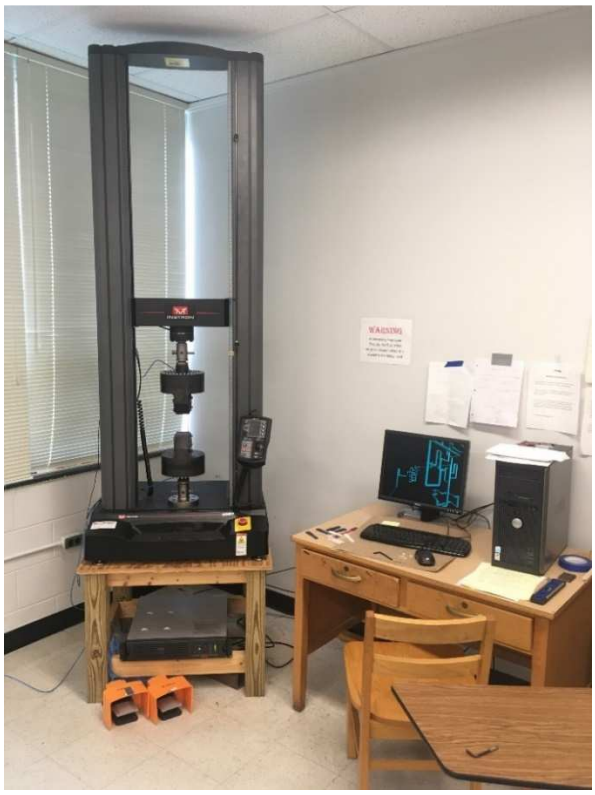

Figure [3.8]: Instron 5967 Universal Testing Machine

3.3 DMLS Energy Density Model

The process parameters investigated in this study are identified after accounting for the amount of energy required to fully sinter each layer of powder in the DMLS build process, this value is known as the energy density and has the units of J/mm^3. This calculation was used for the infill of the part being built. When building parts by AM, there are three main sections that

the part is divided into - infill, up-skin, and down-skin. The down-skin refers to a downward facing angle on the part while the up-skin refers to an angle that is facing up, with regards to the build plate. The infill is everything on the inside of the part. Figure [3.9] shows an image depicting these aspects of a part being built by AM. In this depiction, infill is represented by in-skin. For this study, the number of layers printed with up-skin or down-skin parameters was manually set to zero so the entire part would be printed with the infill settings. This was done to ensure consistent results from the testing phase.

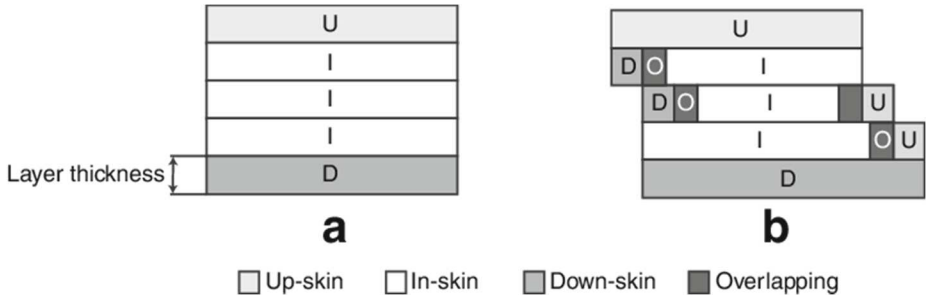

Figure [3.9]: Up-skin, Down-skin, Infill [8]

Energy density is a function of laser power (Watts), laser scan speed (mm/s), layer thickness (mm), and laser hatch distance (mm). The equation for calculating energy density can be expressed as:

$$Energy\ Density = \frac{Laser\ Power}{Scan\ Speed * Layer\ Thickness * Hatch\ Distance} \tag{3.20}$$

Eq. (3.20) is used to determine if the DMLS machine has adequate energy to sinter all the powdered material on each layer of the build. Having an energy density value that is not high enough could result in un-sintered material within the part leading to a reduction in part performance or premature failure upon loading. Each set of parameters used in this study was evaluated by using the energy density calculation to make sure each layer of the part being fully sintered. The parameters that were altered in the Design of Experiments (DOE) for this study are layer thickness, laser scan speed, and laser hatch distance. This leaves laser power as the only parameter not used in the DOE. This was done to have at least one parameter than can be adjusted to maintain adequate energy density. Laser power was adjusted for each print to ensure energy density while keeping all other parameters set to the chosen high and low values for the DOE. This ensures that analyzing the DOE will deliver accurate results when it comes to analyzing the influence of each individual process parameter. The baseline energy density calculated to be around 100 J/mm^3. This value was obtained from running the default parameters through the energy density calculation. For each test run of the DOE, the laser power was adjusted accordingly to stay at this value of 100 J/mm^3. A Table of the default parameters used to get this energy density value can be found in Table [3.3].

Table [3.3]: Default Process Parameters

Power, p (W)	195
Scan Speed, v (mm/s)	1083
Layer Thickness, t (mm)	0.02
Hatch Distance, hd (mm)	0.09
Energy Density, E (J/mm^3)	100.03

3.4 Conclusions

In conclusion, the high cycle fatigue model has been used to develop the fatigue testing machine required for this study. This model has allowed for appropriate selection of the actuator for the geometry chosen for testing. This machine has been controlled by using the LabVIEW software, used in conjunction with a data acquisition device in the form of USB 6009 NI-DAQ. The use of LabVIEW has been crucial since it allows the test to be automated and to be run at the desired frequency. All tests have been conducted at different process parameter values, the results from these test configurations will be presented in Chapter 4. The appropriate energy density for each configuration built from the DMLS machine has been calculated by using the energy density model.

CHAPTER FOUR: EXPERIMENTAL RESULTS

This chapter presents the results obtained for this study. The experimental setup that has been used for all testing is explained and the set up used for data collection is also discussed. The experimental setup includes information on test sample preparation for the direct metal laser sintering (DMLS) process using EOSPRINT and Materialise Magics. A two level, three factor full factorial design of experiments has been used to analyze the results and to determine the influence of individual parameters and parameter interactions, all analysis results are presented in this chapter. A preliminary regression model is also presented, such a model can be useful in determining the significance of each DMLS process parameter.

4.1 Experimental Setup

Test samples built for this study were printed on an EOS M290 direct metal laser sintering system located in the Center for Applied Technology on the campus of Western Carolina University. This build involves multiple steps to fix the position and orientation of the part, this was accomplished by using the Materialise Magics 22.03 3D printing software. An image of the support generation can be found in Figure [4.1]. The block support was chosen to support the under-hanging features of the test sample.

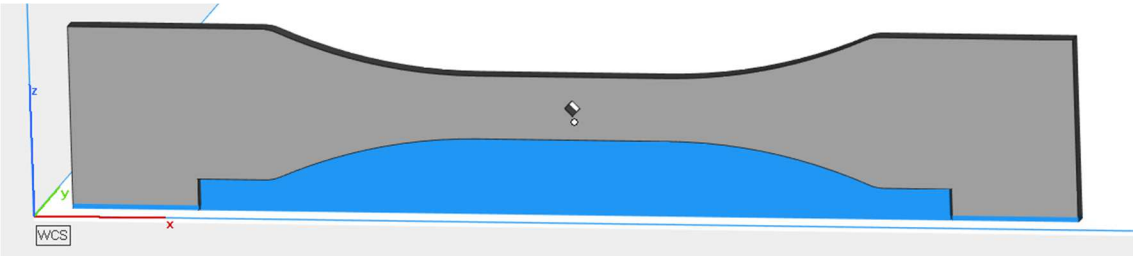

Figure [4.1]: Materialise Magics Pre-Processing

The thin geometry of the test samples requires pins that need to be added to the edges of the dog bone to ensure adequate heat transfer into the build plate. Without these added pins, the part may develop residual stresses that could warp the part upwards and delaminate the part from the build plate. To overcome this issue, the added pins are used to allow the heat to flow through the material into the build plate as opposed to flowing through support material. The support material does not have enough material volume to allow adequate heat transfer. In Figure [4.1], the support material is the blue color while the part is colored gray. Once the test sample has the necessary support added to the part geometry, the next step is to transfer the file to the EOS job and processing management software. Each test sample's parameters were edited using EOSPRINT 2 software. Figure [4.2] shows how the parts were oriented in the processing software, the gold color denotes the part while the purple color denotes the support material.

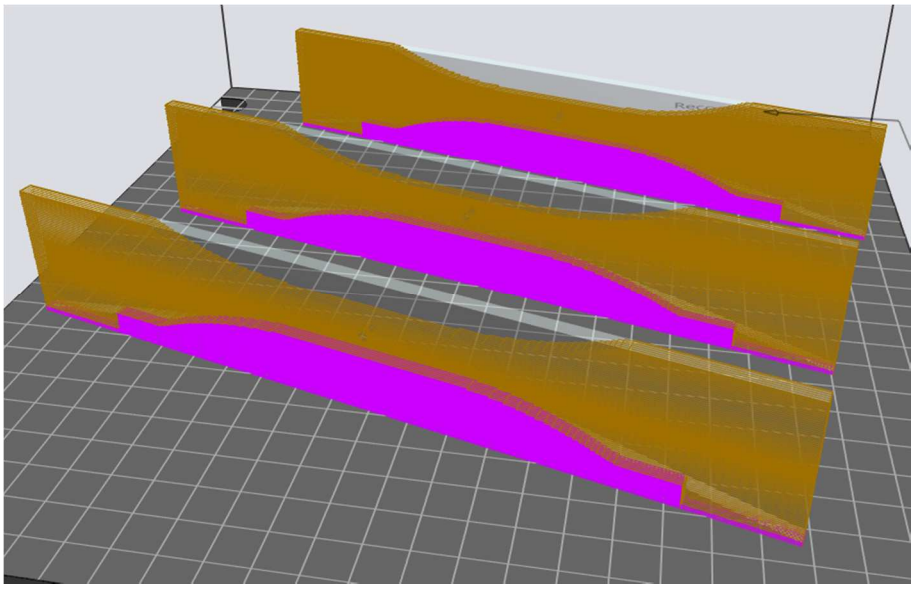

Figure [4.2]: EOSPRINT 2 Test Sample Layout

Each test sample is rotated by 15 degrees to ensure the re-coater blade of the DMLS machine doesn't collide with the part and cause issues with the build. EOSPRINT 2 works as the interface, allowing a simple change of process parameters. Also, this software allows the user to print multiple test samples with different process parameters at the same time. Figure [4.3] shows an image of eight different test samples being printed on the same build plate. Each color represents a part that is being built with a different set of process parameters. It may be noted that if this many test samples are being printed at the same time, it is important to stagger the test samples so that the re-coater blade of the DMLS machine does not collide with all the test samples at the same time, causing issues with the build process.

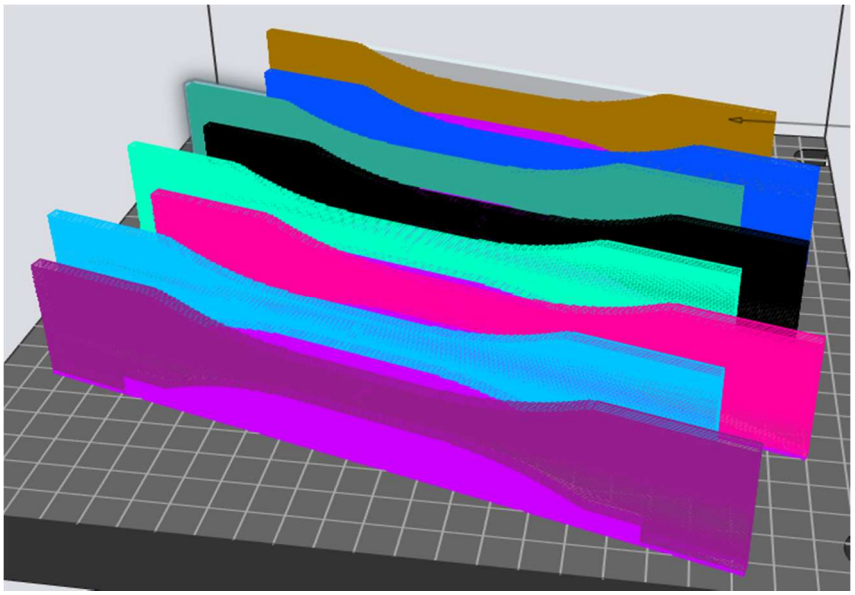

Figure [4.3]: Build plate – multiple samples

After printing, the build plates need to be transferred to a machine shop to remove each test sample from the build plate manually. A horizontal bandsaw was used for this purpose and the support material was manually removed with hand tools. The through hole in the part was printed in the shape of a diamond to ensure that there was no support material needed for this feature in the part. This required post-processing on a drill press with the use of an eighth inch drill bit to machine the through hole.

The post-processed parts are ready for fatigue testing and can be directly tested for high cycle fatigue. An image of the fatigue testing bench and the complete test set up can be seen in Figure [4.4]. At the fatigue testing station, each test sample is tested till failure at a rate of about 2.5 Hz with a load of approximately 60 lbf to ensure that the part fails within the range of 7,000 to 13,000 cycles. Once the test sample fails, the force sensor in the system gets triggered, this automatically stops the test. At the end of the test, the number of cycles to failure is recorded. This process has been repeated for testing all the samples used in this study.

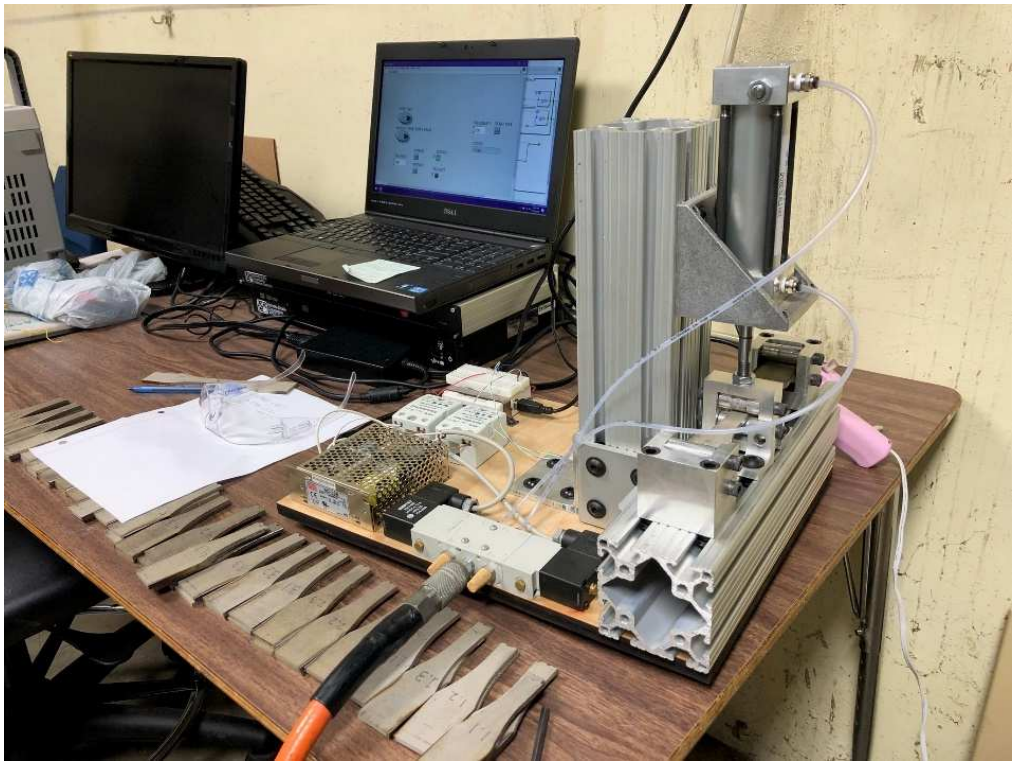

Figure [4.4]: Fatigue Testing Bench

4.2 Design of Experiments

The purpose of using a design of experiments (DOE) in this study is to find out if certain DMLS process parameters are more statistically significant than others for fatigue life. The process parameters that have been used in this DOE include layer height, laser scan speed, and laser hatch distance. These three parameters have been chosen because they can have a significant influence on manufacturing time. The layer height controls the height of each layer of powdered metal that is being recoated onto the build plate during the build process. The scan speed is the speed at which the laser moves when sintering each layer. The final process parameter is the hatch distance of the laser used to sinter each layer. This value equates to how wide the laser beam is when sintering. These process parameters are known to exhibit a strong

influence on the build process. The low settings are selected as the default settings for a standard print recommended by the manufacturer. This has been done to investigate the possibility of increasing these values to reduce the time of the build. Due to limitations set by EOS, the layer thickness can only be incremented by a value of the default thickness. For example, the setting for layer thickness can only be set to 0.02 mm, 0.04 mm, 0.06 mm, etc. For this reason, 0.04 mm has been chosen to be the high setting for layer thickness. The values for scan speed and hatch distance have been selected by using the energy density model discussed in Section 3.3. Using the energy density model, a 370-watt limitation of laser power led to selecting a 15% increase in scan speed and an 11% increase in hatch distance for the high values of these two parameters. Values used in this study can be found in Table [4.1]. Typically, the variables in a DOE are called factors, but for this study the variables or factors are being referred to as parameters in order to keep consistency with DMLS terminology.

Table [4.1]: Process Parameter Levels

Parameter Name	Parameter Letter	Low Setting	High Setting
Layer Thickness	A	0.02 mm	0.04 mm
Scan Speed	B	1083 mm/s	1245 mm/s
Hatch Distance	C	0.09 mm	0.1 mm

Three replicates have been printed and tested for each set of parameters. This equated to a 2^3 full factorial DOE with three replicates that can be used to analyze main effects of each parameter as well as parameter interaction effects. Table [4.2] shows the full DOE matrix used in this study. The cycles to failure (CTF) from all three replicates are also listed in Table [4.2].

Table [4.1] contains the parameters in an un-coded form while the full DOE matrix in Table [4.2] contains the coded and un-coded version of each parameter. The coded version refers to the high (+1) or low (-1) value of each parameter. This is important when discussing the linear regression model later in this chapter.

Table [4.2]: Design of Experiments Matrix

Run Order	Layer Thickness (mm)	Scan Speed (mm/s)	Hatch Distance (mm)	A	B	C	CTF Trial 1	CTF Trial 2	CTF Trial 3
1	0.02	1083	0.09	-1	-1	-1	13798	13800	13559
2	0.04	1083	0.09	1	-1	-1	6823	6335	9196
3	0.02	1245	0.09	-1	1	-1	9278	9917	10396
4	0.04	1245	0.09	1	1	-1	8853	8047	9803
5	0.02	1083	0.1	-1	-1	1	9075	11302	11171
6	0.04	1083	0.1	1	-1	1	7574	7848	8008
7	0.02	1245	0.1	-1	1	1	11143	10556	10610
8	0.04	1245	0.1	1	1	1	7123	8369	8757

Using the data collected in Table [4.2], the results are post-processed by using the statistics software, Minitab, to analyze significant parameters, main effects, and interaction effects. Table [4.3] shows one of the results of the analysis of variance, the p-values for each parameter as well as the two-way and three-way interactions produced with the results from Table [4.2]. This table can be used to determine which parameters, if any, are significant when considering fatigue life for high cycle fatigue. Results from this table can also be used to determine which parameter interactions, if any, may be statistically significant in increasing or decreasing fatigue life.

Table [4.3]: Single Parameter and Parameter Interaction p-Values

Source	p-Value
Model	0.000
Linear	0.000
Layer Thickness	0.000
Scan Speed	0.199
Hatch Distance	0.067
2-Way Interactions	0.004
Layer Thickness*Scan Speed	0.002
Layer Thickness*Hatch Distance	0.208
Scan Speed*Hatch Distance	0.053
3-Way Interactions	0.002
Layer Thickness*Scan Speed*Hatch Distance	0.002

The p-values in Table [4.3] can be analyzed by first selecting a confidence interval. For this study, a confidence interval of 95% has been used. This equates to a significance level, or alpha value, of 0.05. This means that when a p-value for a single parameter or a parameter interaction is below the alpha value of 0.05, it can be concluded that the parameter or interaction is statistically significant for fatigue life with 95% confidence.

The significance of each parameter can be further investigated by observing the main effects plot for each parameter. The main effects plots for each parameter can be found in Figures [4.5], [4.6], and [4.7]. It is important to note that for the sake of comparison, the scale of each graph is manually set to be the same throughout. The significance or insignificance of each parameter can be subjectively evaluated by viewing the slope of the line in the main effects plots. Each line spans from the mean number of cycles to failure at the low value to the mean number of cycles to failure at the high value. The steeper the slope is, the more drastic the change of mean number of cycles to failure (as the parameter changes from low to high). The parameters

deemed statistically significant from Table [4.3] can be qualitatively evaluated by viewing the slope of the main effects plot for the parameter. In general, the higher the slope, the more influential a parameter is expected to be.

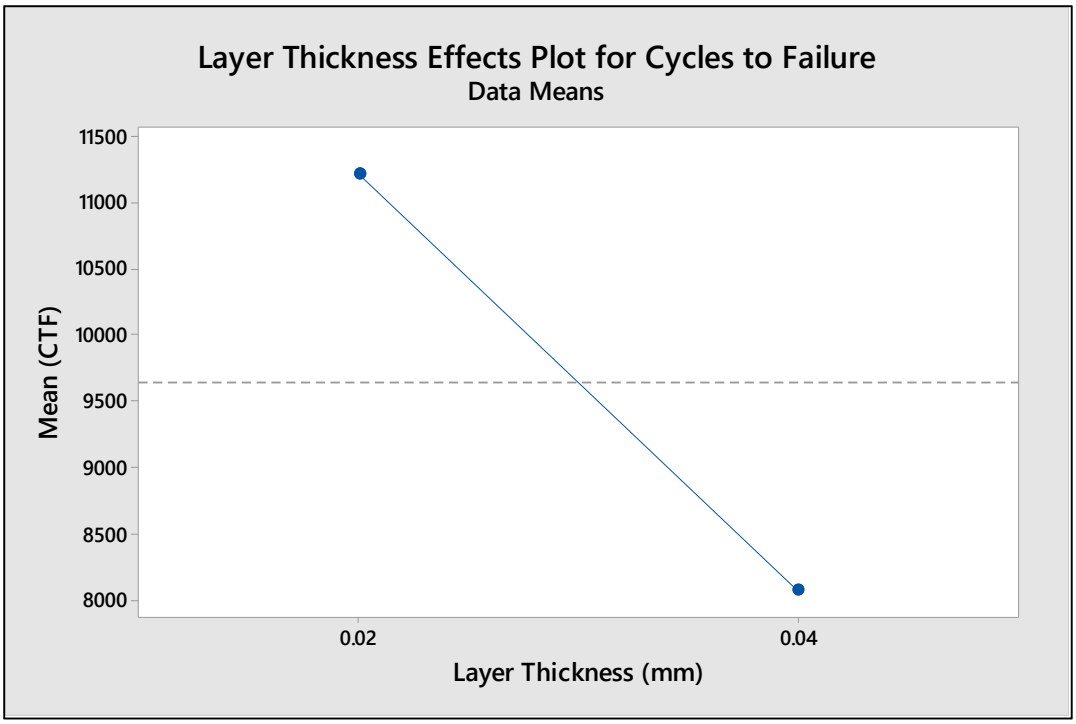

Figure [4.5]: Layer Thickness Main Effects Plot for Cycles to Failure

Table [4.3] shows that layer thickness is determined to be a significant parameter for fatigue life. This is concluded because the p-value for layer thickness is 0.000, which is lower than the alpha value of 0.05 used for this study. The slope for the main effect plot of the layer thickness parameter in Figure [4.5] demonstrates the significance of this parameter since it can be clearly seen that an increase in layer thickness results in a reduction in fatigue life. Compared

to the other main effects plots, the slope of the line for layer thickness is the steepest out of the three. This correlates to the most drastic change in mean cycles to failure when going from the low, the default value on the machine, to the high setting. From the p-value for layer thickness from Table [4.3] and the slope of the line in Figure [4.5], it can be concluded that layer thickness is a statistically significant parameter for fatigue life.

The main effect of scan speed can be seen in Figure [4.6]. Table [4.3] shows that the scan speed parameter is statistically insignificant for fatigue life. This is concluded because the p-value for scan speed is 0.199, which is higher than the alpha value of 0.05 used for this study. The slope for the main effect plot of the scan speed parameter can be seen in Figure [4.6]. It can be seen that this parameter is relatively insignificant since the slope of the line in Figure [4.6] is the flattest out of the three parameters evaluated in this study. From the p-value for scan speed in Table [4.3] and the slope of the line in Figure [4.6], it can be concluded that scan speed is not a statistically significant parameter for fatigue life. It should be noted that this conclusion is limited to the range of values of scan speed (1083 mm/s to 1245 mm/s) investigated in this study.

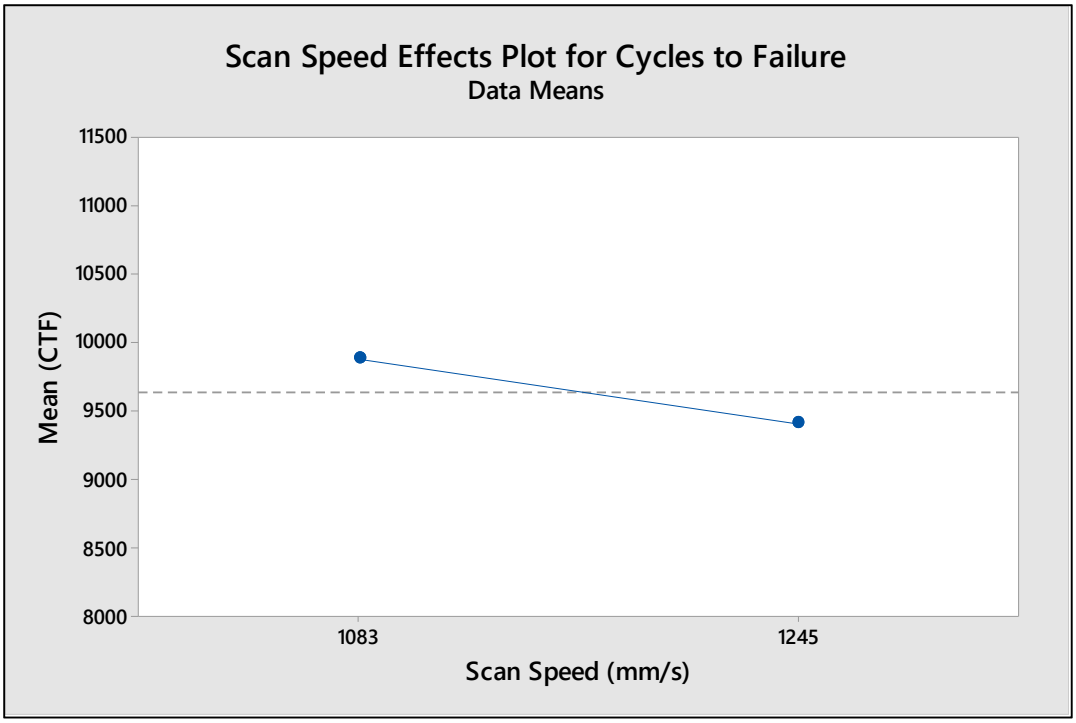

Figure [4.6]: Scan Speed Main Effects Plot for Cycles to Failure

The next, and final, main effect plot for a single parameter is that of hatch distance, and can be found in Figure [4.7]. Table [4.3] shows that hatch distance is a statistically insignificant parameter for fatigue life. This is because the p-value for hatch distance is 0.067, which is slightly higher than the alpha value of 0.05 used for this study. The slope for the main effect plot of the hatch distance parameter in Figure [4.7] demonstrates the relative insignificance of this parameter. The p-value for hatch distance in Table [4.3] and the slope of the line in the main effects plot for hatch distance in Figure [4.7] indicate that this parameter is not statistically significant for fatigue life. It should however be noted that increasing hatch distance seems to result in a reduction in fatigue life. This will need to be investigated further over a larger range of hatch distance.

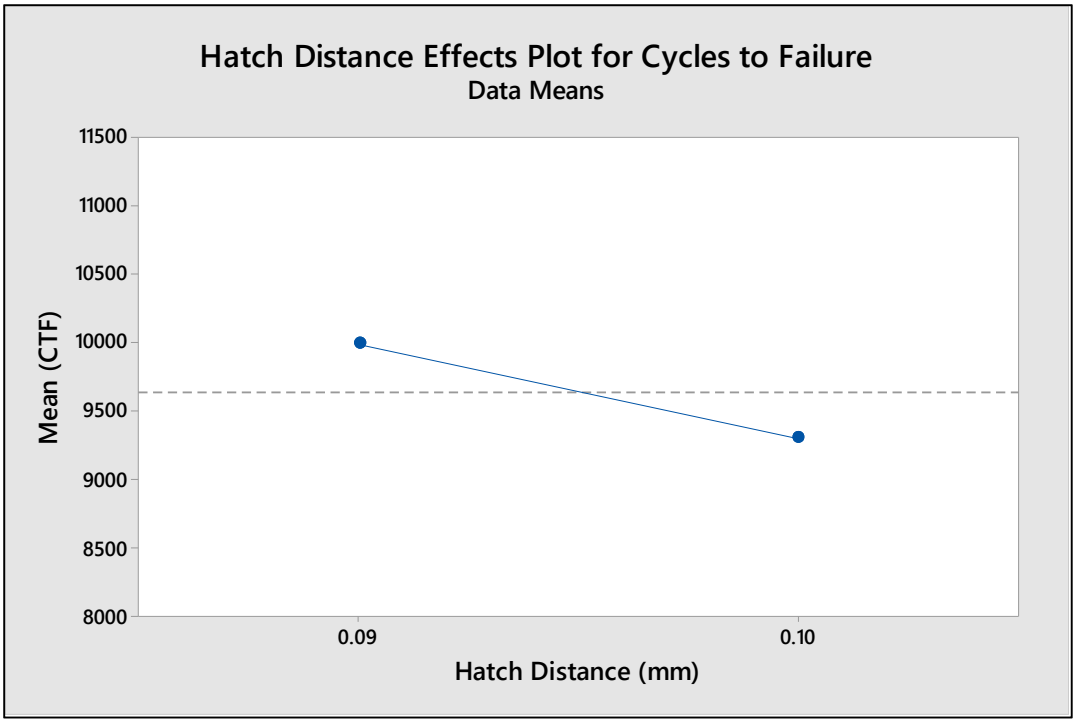

Figure [4.7]: Hatch Distance Main Effects Plot for Cycles to Failure

The interactions between the parameters can be observed from the p-values in Table [4.3] as well as by using interaction plots for each possible combination of parameters. The interaction plots can be found in Figures [4.8], [4.10], and [4.12]. The significance, or insignificance, of each interaction is qualitatively evaluated from the slope of the line in the plot. Parallel lines indicate that there may be very limited interaction between the parameters while non-parallel lines indicate there may be some interaction effect [19]. The greater the interaction effect between two parameters, the greater their influence is on fatigue life.

From Table [4.3], it can be seen that the greatest interaction effect is due to interaction between layer thickness and scan speed with a p-value of 0.002. The interaction plot between layer thickness and scan speed is seen in Figure [4.8] and seems to corroborate the statistical

significance from the p-value. The two lines trend in opposite directions therefore, the interaction between layer thickness and scan speed can be concluded to be statistically significant for fatigue life, with 95% confidence.

To further observe the interaction between layer thickness and scan speed, a three-dimensional plot has also been evaluated, and can be found in Figure [4.9]. From Figure [4.9], it can be seen that at a layer thickness of 0.04 mm, the number of cycles increases when going from a scan speed of 1083 mm/s to 1245 mm/s. At a layer thickness of 0.02 mm, the number of cycles decreases when going from a scan speed of 1083 mm/s to 1245 mm/s. When going from 0.02 mm layer thickness to 0.04 mm layer thickness, the number of cycles decreases regardless of the increase of scan speed. The response of cycles to failure is not consistent throughout the changes of layer thickness and scan speed, therefore it can be concluded that some interaction does take place between these two parameters, although it may be possible that layer thickness dominates this interaction effect. This will need to be investigated further.

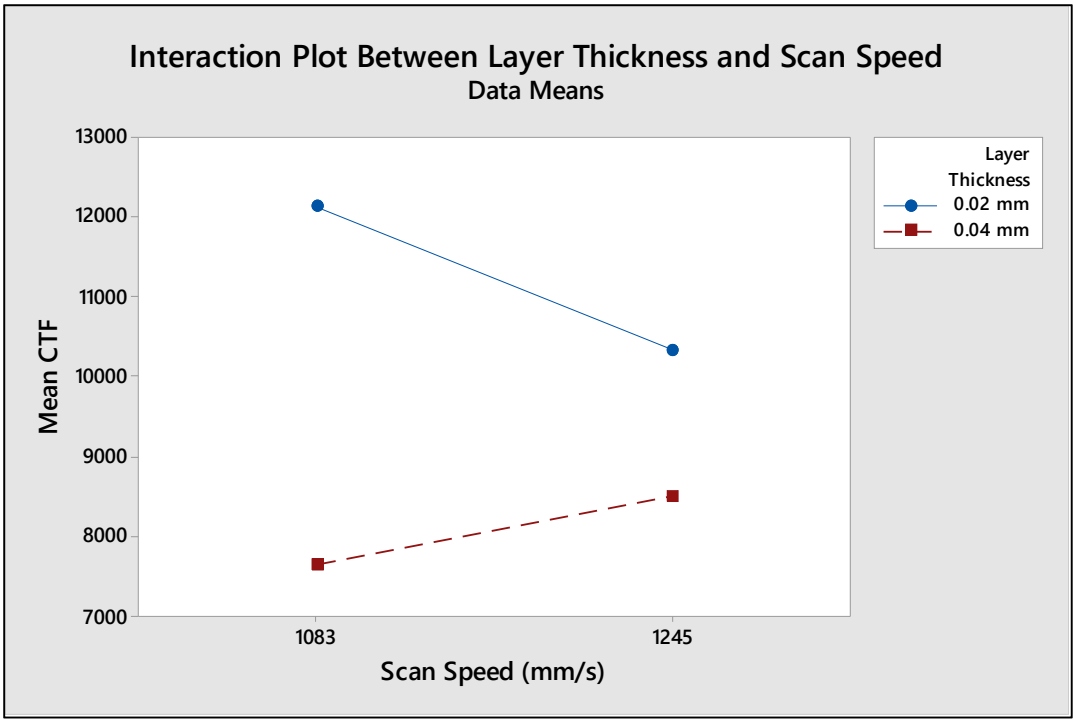

Figure [4.8]: Layer Thickness and Scan Speed Interaction Plot

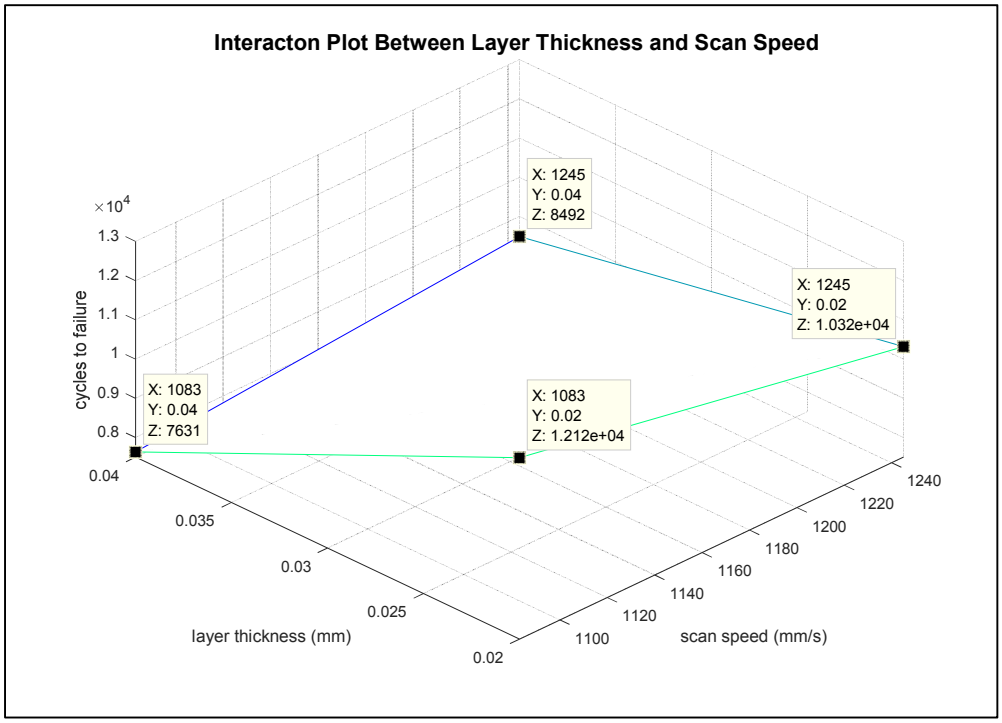

Figure [4.9]: Layer Thickness and Scan Speed 3D Interaction Plot

The next two-way interaction effect observed is that of the interaction between layer thickness and hatch distance, and can be found in Figure [4.10]. The highest two-way interaction p-value observed in Table [4.3] is the interaction between layer thickness and hatch distance. This value of 0.208 is higher than the alpha value selected for this study of 0.05. The interaction plot in Figure [4.10] displays two lines that are almost parallel. Going back to determining the significance of a parameter interaction, the more parallel the two lines are, the more insignificant the interaction can be considered [19]. The two lines in Figure [4.10] trend in the same direction as the hatch distance increases, regardless of the layer thickness, implying no interaction. This observation validates the p-value observed in Table [4.3], so it can be concluded with 95% confidence that the interaction between layer thickness and hatch distance is statistically insignificant for fatigue life.

To further investigate this insignificant interaction, a three-dimensional interaction plot is evaluated, this can be found in Figure [4.11]. In Figure [4.11], at a layer thickness of 0.04 mm, the number of cycles to failure decreases slightly when going from a hatch distance value of 0.09 mm to 0.1 mm. The same occurrence happens when observing the number of cycles to failure at a layer thickness of 0.02 mm and an increase of hatch distance from 0.09 mm to 0.1 mm. When observing the line at a scan speed of 1083 mm/s and increasing from 0.02 mm layer thickness to 0.04 mm layer thickness, the number of cycles to failure increases. The same occurrence happens when observing the line at a scan speed of 1245 mm/s and increasing from 0.02 mm to 0.04 mm layer thickness. This symmetrical trend resembles the parallelism as the interaction plot in Figure [4.10] and helps to conclude that there is no interaction between the parameters of layer thickness and hatch distance.

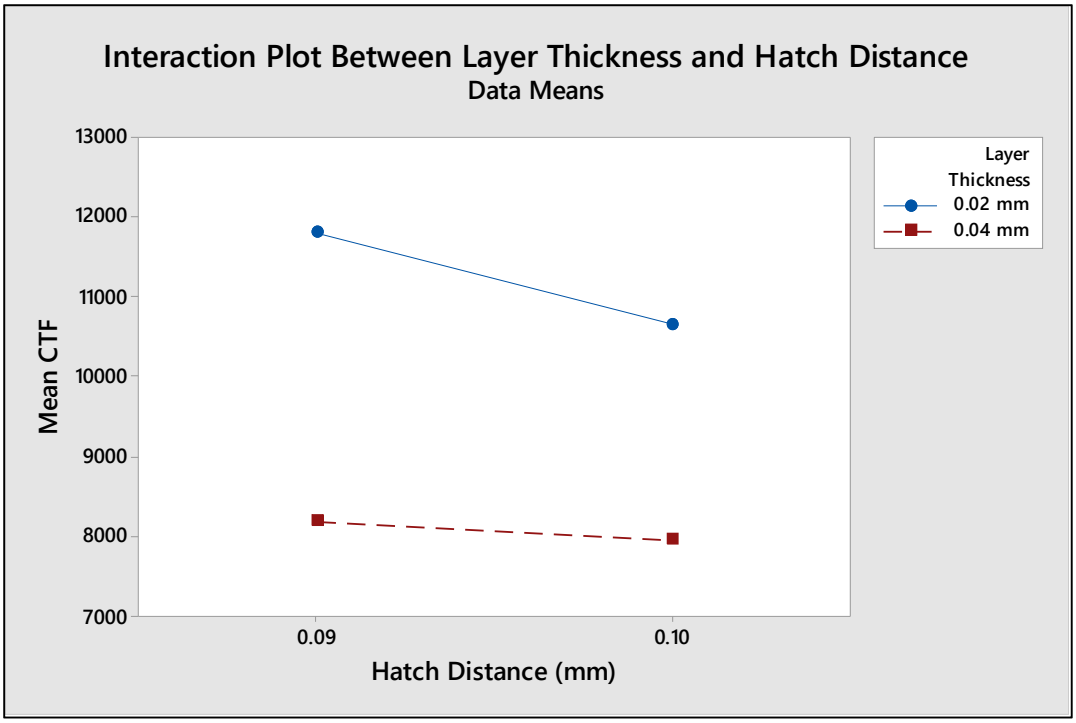

Figure [4.10]: Layer Thickness and Hatch Distance Interaction Plot

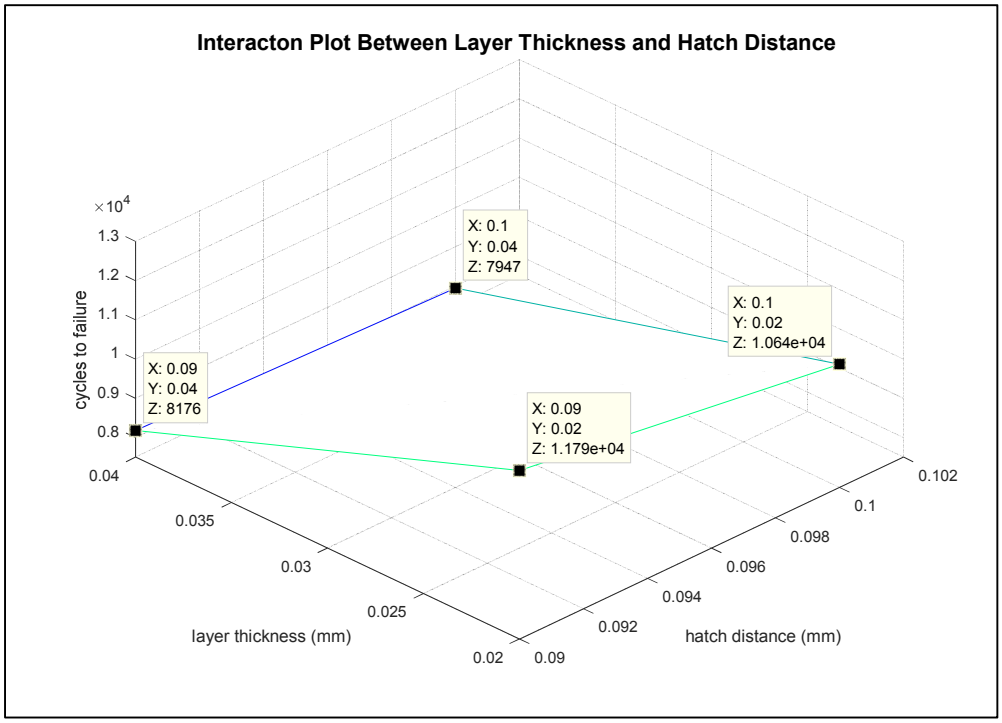

Figure [4.11]: Layer Thickness and Hatch Distance 3D interaction Plot

The final two-way interaction observed is that of the interaction between scan speed and hatch distance, and can be found in Figure [4.12]. The second lowest two-way interaction p-value observed in Table [4.3] is the interaction between scan speed and hatch distance with a p-value of 0.053. This value is very close to being below the alpha value of 0.05 so it can be concluded that with a lower confidence interval, this interaction could possibly be significant. The interaction plot in Figure [4.12] corroborates this statement because the two lines resemble the interaction plot lines for layer thickness and scan speed in Figure [4.8], more than the lines of the interaction plot between layer thickness and hatch distance in Figure [4.10]. Observing the parallelism of the lines in Figure [4.12] and the p-value in Table [4.3], it can be concluded that the two-way interaction between scan speed and hatch distance is statistically insignificant but might need further consideration.

The insignificant interaction between scan speed and hatch distance can be further investigated by observing a three-dimensional interaction plot, as seen in Figure [4.13]. In Figure [4.13], while staying at a scan speed value of 1245 mm/s and increasing the hatch distance value from 0.09 mm to 0.1 mm, the number of cycles to failure decreases a negligible amount. The same cannot be said while staying at a scan speed value of 1083 mm/s. At 1083 mm/s, while increasing the hatch distance from 0.09 mm to 0.1 mm, the number of cycles to failure decreases by much more. When the hatch distance is fixed at a value of 0.09 mm and the scan speed is increased from 1083 mm/s to 1245 mm/s, the number of cycles to failure decreases. The opposite happens when staying at a hatch distance value of 0.1 mm and increasing scan speed. This irregularity in the trend for cycles to failure seems to indicate that there may be some interaction between the two parameters of hatch distance and scan speed, however the results from Table

[4.3] indicate that the interaction is not strong enough to be deemed statistically significant. It is possible that if a lower confidence interval is chosen, this interaction could be significant.

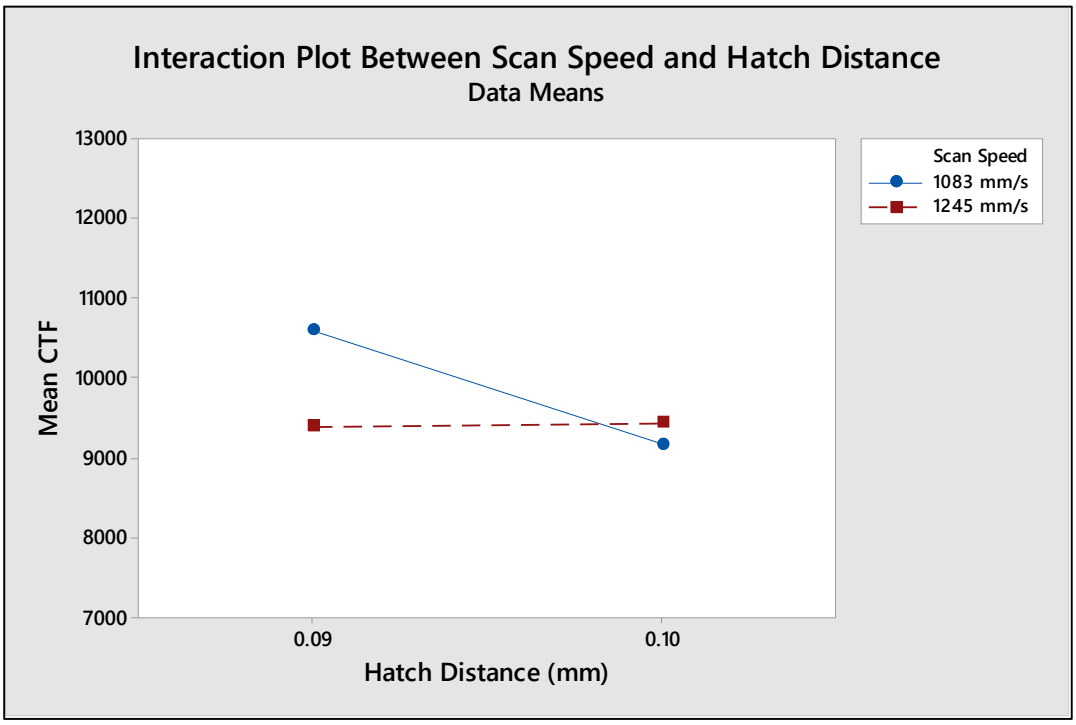

Figure [4.12]: Scan Speed and Hatch Distance Interaction Plot

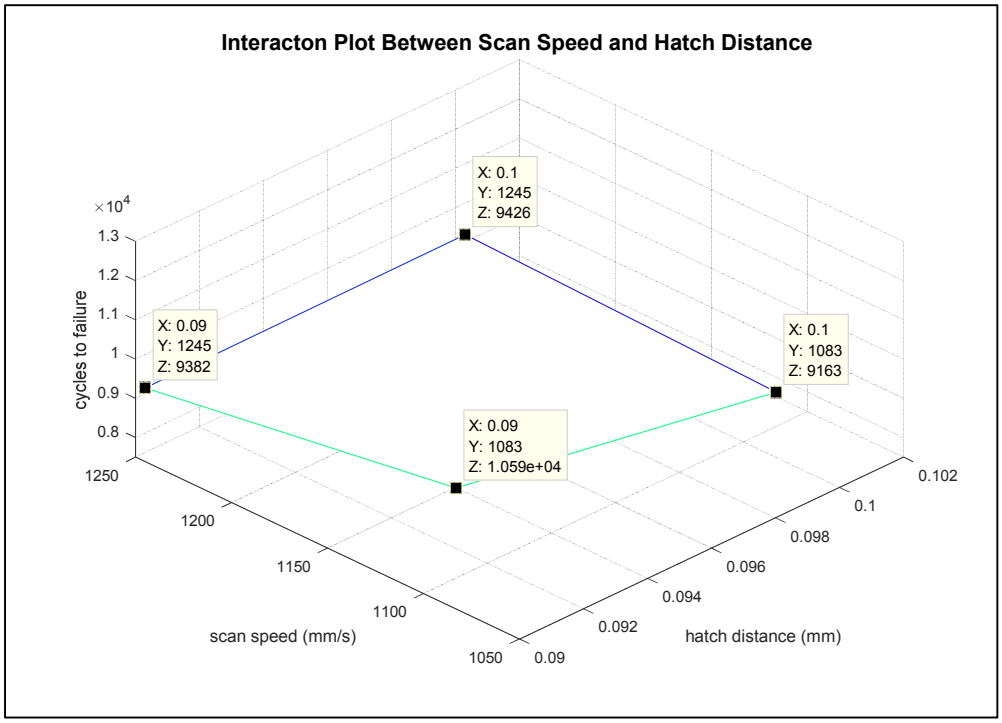

Figure [4.13]: Scan Speed and Hatch Distance 3D Interaction Plot

4.3 Regression Analysis

Data obtained from the DOE has been used to form a linear regression model that can be used to predict cycles to failure with parameters within the domain used in this study. The same statistical software, Minitab, has been used to compute a linear regression model with the data obtained from the design of experiments. The regression equation shown below corresponds to an R^2 value of 88.37%:

$$CTF = 707353 - (19590426 * LT) - (578 * SS) - (6956975 * HD) + (16320 * LT * SS) + (194486636 * LT * HD) + (5799 * SS * HD) - (163138 * LT * SS * HD) \quad (4.1)$$

In Eq. (4.1), *LT* stands for the parameter layer thickness, *SS* stands for the parameter scan speed, *HD* stands for the parameter hatch distance, and *CTF* stands for cycles to failure. Eq. (4.1) contains coefficients that correspond to the un-coded version of the parameters. For example, the first parameter influence that uses the *LT* value multiplied by 19,590,426 uses the desired value for layer thickness (between 0.02 mm or 0.04 mm). This is important to note to understand why the coefficient values are very large, this can be partially attributed to the significantly different scales for the three parameters. For example, while layer thickness ranges from 0.02 mm to 0.04 mm, scan speed is around 1080 mm/s.

This coefficient of determination (R^2) can be used to quantify the fit of the regression model. The higher the value for R^2, the closer the data set is to the linear regression line. Based on the calculated value, it can be said that each of the three parameters has a negative impact on fatigue life. Using the results from the DOE, it can be concluded that layer thickness has the greatest effect out of all parameters tested in this study, as already concluded. All the two-way interactions have a positive impact on fatigue life and the three-way interaction between all parameters tested in this study has a negative impact. This can be seen from the regression equation in Eq. (4.1). It may be noted that a negative coefficient corresponds to a decreased number of cycles to failure while a positive coefficient corresponds to an increased number of cycles to failure.

The regression model has been used to perform validation testing to determine the accuracy of the regression model. This has been done by printing four new test samples with random process parameters within the domain tested in this study. Each validation run contains one replicate. Table [4.4] shows the results from the validation runs as well as the parameters used. The measured values and the predicted values for cycles to failure are also listed in Table [4.4].

Table [4.4]: Regression Model Data

Run	Layer Thickness (mm)	Scan Speed (mm/s)	Hatch Distance (mm)	Measured CTF	Predicted CTF	Percent Error
1	0.02	1115	0.0915	11695	13111	10.80%
2	0.04	1115	0.0915	9582	8274	15.80%
3	0.02	1200	0.0985	13424	11284	18.96%
4	0.04	1200	0.0985	8373	8636	3.05%

As can be seen from the results in Table [4.4], the regression model results are within 3 to 19% of the actual test values. This is a reasonable estimate for high cycle fatigue considering the amount of test samples used in this study. Due to the nature of high cycle fatigue, the scatter of fatigue data generally tends to be high since there is no distinction between crack initiation, crack propagation, and final failure. Test results from high cycle fatigue are expected to have a considerable scatter when only a handful of samples are tested [15]. Each test sample has its own fatigue limit which can vary significantly from sample to sample [15] since high cycle fatigue is determined by a fail or no-fail criteria for the number of cycles to failure. Since this study is

focused on the influence on high cycle fatigue and not a study of DMLS fatigue properties, a high cycle fatigue analysis is considered to be adequate.

4.4 Static Test Results

Tensile testing has been completed by using an Instron universal testing machine. Test samples were machined into uniform cross-sectional samples with rectangular cross-section and pulled in tension until failure. Four different process parameter combinations from Table [4.2] have been used to gather data from tensile testing. Table [4.5] shows the different parameters used in static testing. The test sample number is directly from the runs in Table [4.2].

Table [4.5]: Tensile Testing Sample Parameters

Test Sample Number	Layer Thickness (mm)	Scan Speed (mm/s)	Hatch Distance (mm)
1	0.02	1083	0.09
2	0.04	1083	0.09
5	0.02	1083	0.1
8	0.04	1245	0.1

The selection of each combination involved observing the fatigue life data and selecting four different test samples that correspond to an extreme number of cycles to failure. Test sample number 1 correlates to the parameter combination that yielded the greatest number of cycles to failure while test sample number 2 correlates to the parameter combination that yielded the least number of cycles to failure. Test samples 5 and 8 were selected because of their near median values of cycles to failure. Each parameter combination consists of one tensile test to collect

data. The importance of this test is to verify any process parameter effects on static mechanical properties of printed 316L stainless steel, specifically the ultimate tensile strength since it is a critical property that is used for estimating fatigue life. Table [4.6] displays results from static testing.

Table [4.6]: Static Tensile Test Results

Test Sample Number	Ultimate Tensile Strength, S_{ut} (MPa)
1	654
2	629
5	670
8	624

The material safety and data sheet for EOS 316L stainless steel [17] contains a published ultimate tensile strength of 640 ± 50 MPa. From the results in Table [4.6], it can be seen that all four test samples had an ultimate tensile strength within this range. This observation concludes that there are no significant deviations from the published S_{ut} due to process parameter effects. These results can also be used to highlight the fact that even though the static tensile strength of parts made from DMLS is statistically identical, this is not the case for fatigue.

4.5 Conclusion

The process parameters evaluated in this study have been altered by using EOSPRINT 2.0, a DMLS job and process management software. Materialise Magics 3D printing software has been utilized to generate the required support material for all test samples. An EOS M290

machine has been used to manufacture each test sample and hand tools were used to perform any post-processing to the printed parts. All parts have been tested for high cycle fatigue on the fatigue testing machine that was designed and developed in-house.

The fatigue testing results have been analyzed through a design of experiments. A confidence interval of 95% has been used to check significance of parameters in this study. Out of the three parameters investigated in this study, layer thickness is found to be statistically significant while the other two parameters, scan speed and hatch distance, are found to be statistically insignificant. In terms of the interaction effect, interaction between layer thickness and scan speed has been found to be statistically significant.

Results from tensile testing indicate that ultimate tensile strength (S_{ut}) values did not deviate outside of the tolerance published by EOS in the material safety and data sheet for 316L stainless steel [17]. The value for S_{ut} is important for this study because it is a critical property that is used for estimating fatigue life. As can be seen from Section 3.1.1, the first step in determining fatigue life is to use the published value for S_{ut}.

A linear regression model that can be used to predict the number of cycles with any process parameters within the range tested in this study has been calculated by using Minitab. This regression model is a function of all parameters tested in this study as well as all possible interactions between these parameters. This model has been used to predict the number of cycles to failure, using variables within the domain of this study, and it is observed that predicted results fall between 3 and 19% of the tested values. This is a reasonable estimate for fatigue life considering the sample size and the nature of high cycle fatigue testing.

CHAPTER FIVE: CONCLUSIONS AND FUTURE RESEARCH

A review of the current literature in direct metal laser sintering (DMLS) reveals that there is a lack of understanding of the effects that the different process parameters may have on static and dynamic properties. The literature indicates that DMLS is not being widely used in different manufacturing applications due to a very high build time. This study investigates three parameters associated with the DMLS process that have a significant influence on build time. The effect of these parameters is investigated by evaluating high cycle fatigue of parts made from stainless steel 316L. This chapter provides a summary of the results and some of the main findings.

5.1 Summary

Direct metal laser sintering (DMLS) consists of fusing powdered metal layer by layer with a high-powered laser until each layer is built, forming a final part. Currently, there are only a few industries that use DMLS in their manufacturing line due to the slow build time and complexity of the process. With current DMLS technology, there is a limitation on the parts that can be produced because of the highly complex process involved in building a part. The focus of this research has been on understanding the DMLS process by investigating the process parameters associated with the build process.

Since build time is commonly acknowledged as a big limitation of this manufacturing process, the main parameters that this study focuses on are directly related to build time and consist of layer thickness, laser scan speed, and laser hatch distance. The investigation in this study focuses on the influence of these parameters on fatigue life, specifically high cycle fatigue. High cycle fatigue is important for industrial applications because this type of fatigue life is

characterized by elastically deforming the part for a number of cycles to failure ranging from 10^3 to 10^6 cycles. If a part reaches past 10^6 cycles, it is considered to have infinite life. A three-point bending test set up has been developed to conduct all fatigue testing for this study.

In order to investigate the influence of process parameters on fatigue life, a two-level, three factor design of experiments (DOE) has been used with three replicates. The results of the DOE are analyzed and a linear regression model is developed to estimate the number of cycles to failure for the chosen process parameters. Validation testing is performed to compare the results of tested parts to estimated results from the regression model. A tensile test has also been carried out to evaluate the ultimate tensile strength of test parts made with different process parameters.

5.2 Conclusions

The results from the analysis of the design of experiments indicate that layer thickness has a significant influence on fatigue life. This can be clearly concluded from the results since the average number of cycles to failure is seen to change from 11,217 (with 0.02 mm layer thickness) to 8,061 (with 0.04 mm layer thickness), equating to a 28% reduction in fatigue life. This can be observed in the main effects plot for layer thickness and could be attributed to the reduction in density resulting from relatively larger voids in the part due to larger layer deposition in the build process. Doubling the layer thickness results in almost doubling the energy required to fully sinter each layer. This is done by increasing the power of the sintering laser from a value of 195 watts to 370 watts for most tests. Increasing the layer thickness by this much could potentially lead to small voids inside the part that in turn affect the density of the part. These voids lead to a potential crack nucleation, that propagates with each test cycle to initiate and eventually propagate a crack till final failure. The strong influence of layer thickness is corroborated by statistical results with a significance of more than 99%.

The set up developed for testing in this study used a sensor to stop the test when the deflection in the test sample was excessive. As the test sample started to manifest damage, the deflection in the part was high enough to trigger the sensor and stop the test. For this study, the number of cycles to failure was recorded at this time because once a crack formed, the test sample was considered to have failed, but once the cycles were recorded, the force sensor was turned off and the test was continued till complete failure as the test sample broke into two pieces. The number of cycles it took to propagate the crack from the initial forming to a complete separation of the test sample was vastly different between the test samples with 0.02 mm layer thickness and 0.04 mm layer thickness. The 0.02 mm layer thickness test took about 100 additional cycles to separate the test sample into two pieces while the test samples with 0.04 mm layer thickness took about 500 additional cycles to separate into two pieces. This phenomenon could potentially prove the statement above regarding small voids left in the test sample when the layer thickness is increased. Once the crack formed on the test sample with a 0.02 mm layer thickness, there were minimal voids for the crack to travel through. On the test samples with 0.04 mm layer thickness, it could be concluded that these additional voids cause the crack to stop once it reaches the voids and in turn requires additional cycles to initiate another crack that eventually leads to failure. This could be investigated further by conducting a low cycle fatigue test or by performing a crack propagation analysis.

The scan speed of the laser is seen to have the least effect on fatigue life out of all three parameters investigated in this study. The first observation that proves this conclusion comes from reviewing the p value of 0.199 which is much greater than the significance level of 0.05 used for this study. This implies that the scan speed process parameter is not statistically significant for fatigue life. The same conclusion can be drawn from the main effects plot. The

slope of the line for this parameter is practically flat, indicating that scan speed is not significant regardless of the other parameters. For the manufacturing process, this implies that scan speed could potentially be increased to reduce the build time without compromising the fatigue life of the part. This will need to be further examined beyond the range of values investigated in this study.

Laser hatch distance has been found to be statistically insignificant for fatigue life. However, this parameter could potentially be statistically significant if a lower confidence interval is chosen. It can be concluded that with a lower significance level, this parameter is somewhat significant for fatigue life. The main effects plot for hatch distance provides additional evidence in support of this conclusion. More investigation will be necessary to probe this parameter in more detail and to determine whether a different range of this parameter may be significant for high cycle fatigue.

In addition to the parameter effects, interaction effects have also been analyzed in this study. The first interaction observed is the two-way interaction between layer thickness and scan speed, the p-value for this interaction is 0.002. The p-value for the interaction between layer thickness and scan speed is the lowest, indicating that this interaction is statistically significant. This could be primarily attributed to the significance of layer thickness. However, the interaction of layer thickness with scan speed may need further investigation.

The interaction between scan speed and hatch distance is close to being significant, however this cannot be concluded with 95% confidence since the p-value is 0.053, slightly higher than the significance level of 0.05 used for analysis. With a lower confidence interval, this significance level would increase, making the interaction between scan speed and hatch distance significant. This can be observed from the interaction plot between these two parameters.

Increasing the range between the high and low values for scan speed and hatch distance could potentially aid in determining the statistical significance of this parameter interaction. The interaction effect between layer thickness and hatch distance has been found to be statistically insignificant. This can be concluded from the p-value as well as the subjective evaluation of the interaction plot between the two parameters.

A linear regression model has been developed to predict the number of cycles to failure with the process parameter values within the design domain used in this study. This model has been used to predict fatigue life by printing four test samples with random combinations of process parameters and has been used to compare the predicted fatigue life with the measured fatigue life. The measured fatigue life is found to be within 3 to 19% of the predicted value from the regression model. For high cycle fatigue, this is a reasonable estimate for fatigue life. Due to the nature of high cycle fatigue analysis, it is expected to have a significant scatter in fatigue life data that ranges from 10^3 cycles to 10^6 cycles. This is primarily since there are multiple factors such as material quality, surface finish, type of machining, stress concentrations, etc. that directly contribute toward fatigue life of a part. In order to obtain a more accurate estimate of fatigue life, it may be necessary to detect crack nucleation and crack propagation separately to comprehend the different stages of fatigue failure.

The research questions identified for this study are as follows:

1. Can DMLS be used to manufacture parts that are equivalent to other processes while expediting the manufacturing speed?
2. What process parameters (such as layer thickness, scan speed, laser hatch distance, etc.) can be used to minimize the build time while maintaining the static structural properties of a part?

3. What process parameters can be used to minimize the build time while maintaining the dynamic structural properties of a part?

Upon completion of testing and analysis for this study, the research questions can be answered. It can be concluded that DMLS can be used to manufacture parts that are equivalent to other manufacturing processes. However, it should be noted that process parameters should be chosen carefully to strike a balance between manufacturing time and expected fatigue life. The speed at which a part is produced with conventual processes depends on the complexity of the geometry of the part being produced. For example, if a part requires a mold to be made, the time spent on mold design will be proportional to the complexity of the part. For DMLS, the complexity of the part may not matter as much as a conventional manufacturing process. The time difference between the two methods, however, needs to be carefully evaluated by accounting for post-processing techniques required for a DMLS part. A highly complex part might require a complicated configuration of support material that entails a higher level of difficulty or more post-processing time. The results from this study could potentially help a designer to determine the parameters that can be altered out of the three parameters investigated in this study. For example, increasing the scan speed of the laser during the DMLS process proved to be statistically insignificant for fatigue life and could potentially lead to a poor surface finish in the part, but it may be viable to increase scan speed to shorten the build time if the part does not need to have a good surface finish for a specific application. It may be necessary to investigate the effect of increasing the scan speed to almost double the default value, which is possible with a 400-watt laser DMLS system.

Results from this study conclude that out of the three parameters (layer thickness, scan speed, and hatch distance), none of them had a significant effect on static material properties such as ultimate tensile strength. Each tensile test sample contained a different combination of process parameters and all test samples yielded nearly identical ultimate tensile strength values. It is important to note that ultimate tensile strength values collected from tensile testing fell within the domain of the ultimate tensile strength published by EOS for 316L stainless steel. However, dynamic testing showed that process parameters have a strong influence on fatigue life.

Out of the three process parameters tested in this study, it can be concluded that the only parameters that can be adjusted to increase build time without significantly affecting fatigue life of the part are scan speed and hatch distance. Layer thickness is found to be statistically significant for fatigue life, increasing layer thickness is found to result in a reduction in fatigue life. Scan speed is found to be least significant for fatigue life. Considering the energy density model used for this study, while staying at a layer thickness of 0.02 mm, the scan speed can potentially be doubled from the default value of 1083 mm/s to 2166 mm/s while maintaining an adequate energy density if the laser power is increased from 195 watts to 370 watts. This can expedite the building process without sacrificing structural dynamic properties. The same could be stated about hatch distance as well. The results from this study conclude that hatch distance is somewhat significant for fatigue life. Further investigation would be necessary to determine the statistical significance of laser scan speed and laser hatch distance.

5.3 Future Work

The scope of research carried out in this study can be enhanced to gain a greater understanding of the process parameters or parameter interactions on high cycle fatigue life for

parts made from DMLS. The first study that could be done is to further investigate different levels of process parameters. Since this study concluded that a higher layer thickness has a negative effect on fatigue life, a larger design of experiments study could be performed to determine other parameters that may be able to overcome the negative influence of higher layer thickness. This will allow the DOE to have a wider range between the high and the low values for scan speed and hatch distance or possibly more process parameters that directly influence build time. The levels selected in this study have been limited due to the limitations in energy density at 0.04 mm layer thickness. By staying at a 0.02 mm layer thickness, the values for scan speed and hatch distance can be increased drastically, while still maintaining the correct energy density. This will specifically allow an in-depth examination of hatch distance and scan speed.

Another study that can be performed with the results of this research could potentially be a crack propagation analysis to further investigate the phenomenon of the differences in crack nucleation and crack propagation with changing layer thickness. The analysis in this study has been limited to high cycle fatigue to study failure when the part breaks. A crack propagation analysis can be beneficial to determine the actual stage of damage that is most affected by a change in layer thickness. This may require some analysis by using low cycle fatigue. Low cycle fatigue will allow an investigation into crack nucleation, crack propagation and final failure.

The approach adopted in this study can also be used to investigate the influence of process parameters in the presence of combined loading. This study has been limited to testing under bending load within a limited range of cycles to failure. This is primarily due to limitations of the test set up and equipment. In order to investigate the influence of parameters holistically, it will be beneficial to understand the impact of process parameters under complex loading conditions.

REFERENCES

[1] B. Wang, "Additive Manufacturing – Direct Laser Sintering of Titanium and other Metals," Next Big Future, 5 April 2010. [Online]. Available: https://www.nextbigfuture.com/2010/04/additive-manufacturing-direct-laser.html. [Accessed 2017].

[2] O. Scott-Emuakpor, J. Schwartz, T. George, C. Holycross, C. Cross and J. Slater, "Bending fatigue life characterisation of direct metal laser sintering nickel alloy 718," *Fatigue & Fracture of Engineering Materials & Structures,* vol. 38, pp. 1105-1117, 2015.

[3] E. Brandl, U. Heckenberger, V. Holzinger and D. Buchbinder, "Additive manufactured AlSi10Mg samples using Selective Laser Melting (SLM): Microstructure, high cycle fatigue, and fracture behavior," *Materials and Design,* vol. 34, pp. 159-169, 2012.

[4] D. Buchbinder, H. Schleifenbaum, S. Heidrich, W. Meiners and J. Bultmann, "High Power Selective Laser Melting (HP SLM) of Aluminum Parts," *Physics Procedia ,* vol. 12, pp. 271-278, 2011.

[5] T. Wohlers and T. Gornet, "History of Additive Manufacturing," Wohlers Associates, Inc., 2016. [Online]. Available: https://www.wohlersassociates.com/history2016.pdf.

[6] D. H. Smith, J. Bicknell, L. Jorgensen, B. M. Patterson, N. I. Cordes, I. Tsukrov and M. Knezevic, Microstructure and Mechanical Behavior of Direct Metal Laser Sintered Iconel Alloy 718, New Mexico: ELSEVIER, 2016.

[7] M. Nozar, I. Zetkova, P. Hanzl and M. Dana, "A CUSTOMER'S VIEW ON KEY ASPECTS OF METAL ADDITIVE MANUFACTURING," in *DAAAM International*, Vienna, Austria, 2017.

[8] F. Calignano, D. Manfredi, E. Ambrosio, L. Iuliano and P. Fino, "Influene of process parameters on surface roughness of aluminum parts produced by DMLS," *The International Journal of Advanced Manufacturing Technology,* vol. 67, no. 9-12, pp. 2743-2751, 2013.

[9] D. C. Summers, Quality, 3rd ed., Prentice Hall, 2003, pp. 525-528.

[10] G.-J. Park, Analytic Methods for Design Practice, 1 ed., Springer-Verlag London, 2007, pp. 309-310.

[11] D. Bingham and V. N. Nair, Noise Variable Settings in Robust Design Experiments, vol. 54, Taylor & Francis, LTD on behalf of American Statisitcal Association and American Society for Quality, 2012, pp. 388-397.

[12] K. Kumari and S. Yadav, Linear Regression Analysis Study, New Delhi, India: Journal of the Practice of Cardiovascular Sciences, 2018.

[13] G. Franceschini and S. Macchietto, Model-based design of experiments for parameter precision: State of the art, South Kensington Campus, London: ELSEVIER, 2007, pp. 4846-4872.

[14] ASTM, *Standard Practice for Controlled Amplitude Axial Fatigue Tests of Metallic Materials,* 1 ed., vol. 3, Philadelphia, PA: American Society for Testing of Materials, 2015.

[15] G. Dieter, Mechanical Metallurgy, McGraw-Hill Book Company, 1961.

[16] J. Essick, Hands-On Introduction to LabVIEW, 3rd ed., Oxford University Press, 2016.

[17] EOS GmbH - Electro Optical Systems, *EOS StainlessSteel 316L Material data sheet,* EOS GmbH, 2014.

[18] R. G. Budynas and J. K. Nisbett, Shigley's Mechanical Engineering Design, 9th ed., McGraw-Hill Companies, Inc., 2011.

[19] J. H. Zar, Biostatistical Analysis, 4th ed., Upper Saddle River, Nj: Prentice-Hall, 1999.

[20] ASTM, *Standard Test Methods for Tension Testing of Metallic Materials,* West Conshohocken, PA: American Society for Testing of Materials, 2016.

[21] P. Hanzl, M. Zetek, T. Bakša and T. Kroupa, The Influence of Processing Parameters on the Mechanical Properties of SLM Parts, Pilsen, Czech Republic: Elsevier Ltd., 2015.